



Norwegian University of  
Science and Technology

# 2D Petroleum System Modelling of two Seismic lines in the Western Part of the Hammerfest Basin

**Adam Abdulla Makame**

Petroleum Geosciences

Submission date: August 2017

Supervisor: Stephen John Lippard, IGP

Norwegian University of Science and Technology  
Department of Geoscience and Petroleum





## **ACKNOWLEDGEMENT**

I would like to acknowledge my main supervisor Professor Stephen John Lippard of the Department of Geoscience and Petroleum (IGP) for his guidance, advice and useful comments throughout the period of this study. The work would not have been possible without the considerable contribution made by him.

Secondly, I would like to give thanks to my co-supervisor from University of Dar es Salaam, Dr. Elisante Mshiu for his encouragement and correction during the period of preparing this work.

I also owe many thanks to Bahati Mohamed, Vicent Mosha and Iddi Mchomvu for their assistance in using Petrel and PetroMod. Many thanks go to Schlumberger for providing the Petrel and PetroMod softwares and academic license to the UDSM Geology department.

## **ABSTRACT**

The study focuses on 2D basin modelling of the Hammerfest Basin to understand the petroleum system of the western part of the Hammerfest Basin and how it was affected by uplift and erosion that occurred during Cenozoic time. Two interpreted seismic sections BSS01-104 and BSS01-106 were loaded in PetroMod software for modelling the petroleum system of the area.

The petroleum system of the Hammerfest Basin consists of source rocks of Middle to Late Triassic (Snadd and Kobbe Formations) and Late Jurassic to Early Cretaceous ages (Hekkingen Formation). Reservoir rocks are of Early to Middle Jurassic age (Sto and Tubaen Formations) and the seal rocks are of Middle to Late Jurassic age (Fuglen Formation), Late Jurassic to Early Cretaceous (Hekkingen Formation) and Lower Cretaceous shales. The maturity indicators, such as temperature, vitrinite reflectance and transformation ratio, were used to determine the maturity of the source rocks.

The Triassic potential source rocks (Snadd and Kobbe Formations) of the area are highly matured and have generated large quantities of hydrocarbons. The Hekkingen Formation of Late Jurassic to Early Cretaceous age is also considered as a potential source rock but it is not matured enough. The modelling shows that the deeper source rocks of Triassic age have generate significant amounts of hydrocarbons, but the upper source rocks of Late Jurassic to Early Cretaceous continue to generate hydrocarbons (both oil and gas) to the present day.

The model has incorporated three phases of erosion. The first phase of erosion took place during 75 to 60 Ma in the Late Cretaceous which eroded 200 m of the Kveite Formation and the second phase took place during 40 to 35 Ma in the Paleogene which eroded 300 m of Torsk Formation and the third phase was between 3.5 to 0.01 Ma in the Neogene which was eroded a further 500 m of Torsk Formation. Therefore, a total of 1000 m thickness of erosion has been modelled.

# TABLE OF CONTENTS

<b>ACKNOWLEDGEMENT</b> .....	<b>i</b>
<b>ABSTRACT</b> .....	<b>ii</b>
<b>TABLE OF CONTENTS</b> .....	<b>iii</b>
<b>LIST OF FIGURES</b> .....	<b>v</b>
<b>LIST OF TABLES</b> .....	<b>vi</b>
<b>Chapter 1</b> .....	<b>1</b>
<b>1.0 INTRODUCTION</b> .....	<b>1</b>
1.1. Location of the Study Area .....	1
1.2. Basin and Petroleum System Modelling .....	2
1.3. Problem Statement .....	3
1.4. Previous Studies .....	3
1.5. Objectives of the Study .....	4
<b>Chapter 2</b> .....	<b>5</b>
<b>2.0 GEOLOGY OF THE STUDY AREA</b> .....	<b>5</b>
2.1. Regional Geology .....	5
2.2. Lithostratigraphy of the Hammerfest Basin.....	6
2.3. Geological Evolution .....	8
2.3.1. Carboniferous .....	8
2.3.2. Late Carboniferous to Early Permian .....	8
2.3.3. Late Permian.....	9
2.3.4. Early–Late Triassic (Induan–Early Norian) .....	9
2.3.5. Late Triassic–Middle Jurassic .....	10
2.3.6. Late Jurassic–Early Cretaceous .....	11
2.3.7. Late Cretaceous .....	12
2.3.8. Cenozoic .....	12
<b>Chapter 3</b> .....	<b>14</b>
<b>3.0 HAMMERFEST BASIN PLAYS</b> .....	<b>14</b>
3.1. Hydrocarbon Source Rocks .....	14
3.1.1. Hekkingen Formation .....	14
3.1.2. Snadd Formation.....	14
3.1.3. Kobbe Formation.....	15

3.2. Reservoir Rocks .....	15
3.2.1. Sto Formation .....	15
3.2.2. Tubaen Formation.....	15
3.3. Seals/Cap Rocks.....	16
3.3.1. Fuglen Formation .....	16
3.3.2. Hekkingen Formation .....	16
3.4. Traps .....	16
<b>Chapter 4 .....</b>	<b>17</b>
<b>4.0 METHODOLOGY .....</b>	<b>17</b>
4.1. Data Compilation .....	18
4.2. Velocity Model Creation.....	18
4.3. Time to Depth Conversion.....	19
4.4. Interpreted Seismic Section reflectors Observation.....	20
<b>Chapter 5 .....</b>	<b>23</b>
<b>5.0 2D BASIN MODELLING.....</b>	<b>23</b>
5.1. Software .....	23
5.2. Data Input.....	24
5.3. Fault Properties Definition.....	26
5.4. Age Assignment.....	28
5.5. Facies Definition.....	30
5.6. Boundary Conditions .....	32
5.7. Model Simulation.....	37
<b>Chapter 6 .....</b>	<b>38</b>
<b>6.0 MODELLING RESULTS AND DISCUSSION.....</b>	<b>38</b>
6.1. Burial History, Erosion and Uplift.....	38
6.2. Source Rock Maturity .....	47
6.3. Hydrocarbon Generation, Migration and Accumulation .....	53
<b>Chapter 7 .....</b>	<b>56</b>
<b>7.0 CONCLUSION .....</b>	<b>56</b>
<b>REFERENCES.....</b>	<b>57</b>
<b>APPENDICES .....</b>	<b>64</b>

## LIST OF FIGURES

Figure 1.1 Location Map of the Barents Sea showing the Hammerfest Basin in the red square, well location and main structural elements (Modified from Ohm et al., 2008).....	1
Figure 1.2 The petroleum system elements (Modified from Magoon and Dow, 1994). ....	2
Figure 2.1 Lithostratigraphy of the Hammerfest Basin with informal units (modified from Dalland et al. 1988).....	7
Figure 4.1 2D seismic lines BSS01-104 and BSS01-106 used in basin modelling. ....	17
Figure 4.2 Synthetic generation window showing interval velocity of the interpreted horizons, which are used for velocity model creation. ....	18
Figure 4.3 Depth converted seismic section BSS01-104 and two wells located at the section. ..	20
Figure 5.1 2D Modelling workflow. ....	24
Figure 5.2 Pre-grid model view of the digitized horizons and faults and layer splitting for model line 104 (In interpreted section only 13 layers can be seen, due to layer splitting 16 layers can be seen in this figure).....	25
Figure 5.3 Pre-grid model view of the digitized horizons and faults and layer splitting for model 106 (In interpreted section only 13 layers can be seen, due to layer splitting 16 layers can be seen in this figure).....	26
Figure 5.4 Sediment Water Interface Temperature (SWIT) definition.....	33
Figure 5.5 Boundary conditions trends for model 104. ....	36
Figure 5.6 Boundary conditions trends for model 106. ....	37
Figure 6.1 250-230 Ma, Orret Formation deposited at Early Triassic layer.....	39
Figure 6.2 230-210 Ma, Kobbe Formation deposited at Middle Triassic layer.....	39
Figure 6.3 210 - 200 Ma, Snadd Formation deposited at Middle to Upper Triassic layer. ....	40
Figure 6.4 200 - 196 Ma, Fruholmen Formation deposited at Upper Triassic layer. ....	40
Figure 6.5 196 - 184Ma, Tubaen Formation deposited at Lower Jurassic layer. ....	41
Figure 6.6 184 - 167 Ma, Nordmela Formation deposited at Lower to Middle Jurassic layer....	41
Figure 6.7 167- 155 Ma, Sto Formation deposited at Middle Jurassic layer. ....	42
Figure 6.8 155 – 140 Ma, Fuglen Formation deposited at Middle to Upper Jurassic layer. ....	42
Figure 6.9 140 – 130 Ma, Hekkingen Formation deposited at Upper Jurassic to Lower Cretaceous layer.....	43
Figure 6.10 130 – 120 Ma, Knurr Formation deposited at Lower Cretaceous 1 layer. ....	43
Figure 6.11 120 – 96 Ma, Kolje Formation deposited at Lower Cretaceous 2 layer.....	44
Figure 6.12 96 – 75 Ma, Kolmule Formation deposited at Lower Cretaceous 3 layer.....	44
Figure 6.13 75 - 60 Ma, first erosion (uplift) of Kveite-Kviting Formation at Late Cretaceous layer, resulting in reduction of layer thickness of 200 m at Late Cretaceous. ....	45
Figure 6.14 40-35 Ma, second erosion (uplift) of Base Paleocene layer, resulting in the reduction of layer thickness of 300 m at Paleocene.....	45
Figure 6.15 3.5 – 0.01 Ma, third erosion (uplift) of Base Quaternary layer, resulting in the reduction of layer thickness of 500 m at Paleogene. ....	46
Figure 6.16 2.5 – 0.01 Ma, Deposition of the Quaternary layer. ....	46
Figure 6.17 0.00 Ma, Present day basin configuration. ....	47
Figure 6.18 Present day temperature of the source rocks intervals for model 104.....	48



Figure 6.19 Present day temperature of the source rocks intervals for model 106.....	49
Figure 6.20 Present day Easy Ro converted in oil and gas generation windows for model 104.	49
Figure 6.21 Present day Easy Ro converted in oil and gas generation windows for model 106.	50
Figure 6.22 Present day transformation ratio for model 104.....	51
Figure 6.23 Present day transformation ratio for model 106.....	51
Figure 6.24 Present day remaining kerogen bulk for model 104.....	52
Figure 6.25 Present day remaining kerogen bulk for model 106.....	52
Figure 6.26 Event chart.....	53
Figure 6.27 Oil upward migration from the source rocks into the reservoirs and the lateral migration within the source rocks.....	54
Figure 6.28 Gas upward migration from the source rocks into the reservoirs and the lateral migration within the source rocks.....	55

## LIST OF TABLES

Table 4.1 Parameters used to create the velocity model.....	19
Table 4.2 Depth converted seismic lines which can be used for 2D modelling.....	20
Table 5.1 Faults properties definition table for model 104.....	27
Table 5.2 Faults properties definition table for model 106.....	28
Table 5.3 Age assignment table for model 104.....	29
Table 5.4 Age assignment table for model 106.....	30
Table 5.5 Facies definition table for model 104.....	31
Table 5.6 Facies definition table for model 106.....	32
Table 5.7 Boundary conditions for model 104.....	34
Table 5.8 Boundary conditions for model 106.....	35

# Chapter 1

## 1.0 INTRODUCTION

### 1.1. Location of the Study Area

The Hammerfest Basin is located in the southwest part of the Barents Sea shelf (Fig. 1.1). It is shallow basin and has an ENE-WSW trend. The basin is separated from the Finnmark Platform to the south by the Troms-Finnmark Fault Complex (TFFC) and from the Loppa High to the north by the Asterias Fault Complex (AFC). Its western limit towards the Tromsø Basin is defined by the southern segment of the Ringvassøy-Loppa Fault Complex (RLFC), whereas its eastern border has the nature of a flexure towards the Bjarmeland Platform (Gabrielsen et al., 1990).

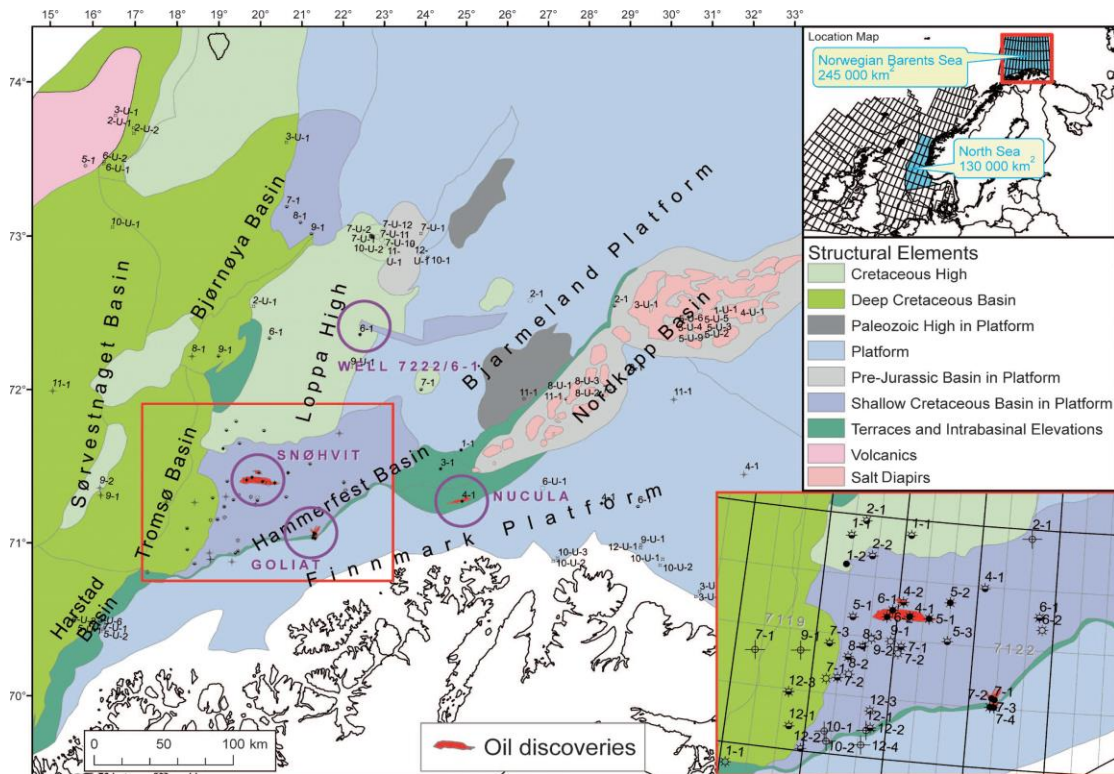


Figure 1.1 Location Map of the Barents Sea showing the Hammerfest Basin in the red square, well location and main structural elements (Modified from Ohm et al., 2008).

The circles on figure 1 show the major discoveries in the area. The top right map shows the relative sizes of the Norwegian Barents Sea (245,000 km<sup>2</sup>) and North Sea (130,000 km<sup>2</sup>).

## 1.2. Basin and Petroleum System Modelling

A petroleum system is a geologic system that encompasses the hydrocarbon source rocks and all related oil and gas accumulations and which includes all of the geologic elements and processes that are essential for a hydrocarbon accumulation to exist (Magoon and Dow, 1994) (Fig. 1.2).

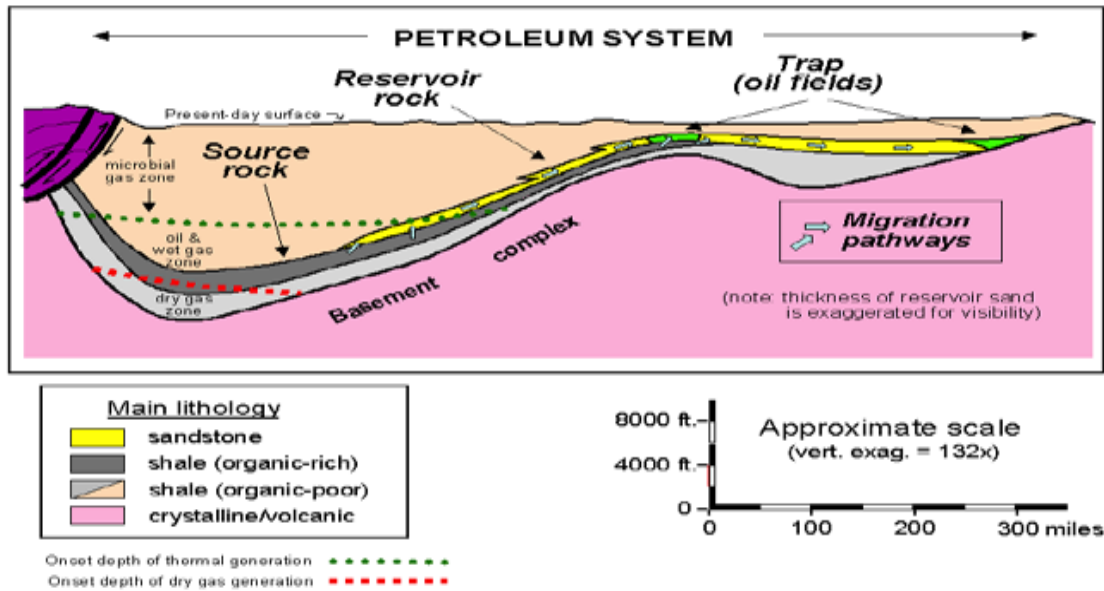


Figure 1.2 The petroleum system elements (Modified from Magoon and Dow, 1994).

A petroleum system model is a digital data model of a petroleum system in which the interrelated processes and their results can be simulated in order to understand and predict them (Hantschel and Kauerauf, 2009). Basin modeling is dynamic modeling of geological processes in sedimentary basins over geological time spans (Hantschel and Kauerauf, 2009). The geological processes calculated and updated at each step include deposition, erosion, compaction, expulsion, phase dissolution, hydrocarbon generation, accumulation and migration. These processes are simulated in a dynamic petroleum systems model in the assessments of exploration risks, migration scenarios and drainage areas. The model seeks to answer questions such as whether hydrocarbons have been generated, where they have been generated, when they were generated, the properties of the hydrocarbons generated and the prospects the hydrocarbons have migrated into.

2D basin modelling has been done for the plays in the Hammerfest Basin using Petromod software. The plays consist of source rocks (Snadd and Kobbe Formations) of Triassic age and (Hekkingen Formation) of Late Jurassic to Early Cretaceous age, a reservoir (Sto and Tubaen Formations) of Early to Middle Jurassic age and seals (Fuglen and Hekkingen Formations) of Middle to Late Jurassic and Late Jurassic to Early Cretaceous ages.

### **1.3. Problem Statement**

The evolution of the Hammerfest Basin through various tectonic and depositional events caused the distribution and development of the petroleum system. Erosion and uplift which occurred late in the basin history (Cenozoic) reduced the temperature that has a strong influence on the maturity of the source rocks, hence affects the generation of the hydrocarbons within the area. However, although there have been several important discoveries within the area, the number of dry wells which were encountered during exploration in the Hammerfest Basin might be due to these events.

### **1.4. Previous Studies**

Various studies have been conducted in the Hammerfest Basin to provide information and knowledge about basin formation, geological activities and petroleum system elements. Some of the studies conducted in the Hammerfest Basin are:

Rodrigues Duran et al. (2013) conducted 3D modelling of the Hammerfest Basin (southwestern Barents Sea). They assessed petroleum generation, migration and leakage during the basin formation. The source rock maturity (vitrinite reflectance) and present day temperature were used to calibrate the model. The maturity levels of the main source rocks (Kobbe, Snadd and Hekkingen Formations) were reconstructed and showed that the highest maturities have been reached in the western and northwestern margins of the basin.

2D Basin Modelling and Petroleum systems analysis of the Triassic Play in the Hammerfest Basin of the Norwegian Barents Sea was carried out by Ben Awuah et al. (2013). Their study enhanced the understanding of the Triassic play in the Hammerfest Basin. The model involves three episodes of erosion (uplift). These episodes of erosion have increased exploration risks in the Hammerfest Basin. Their study showed that the Upper Jurassic Hekkingen Formation is a good source rock rich in organic matter with high values of hydrogen index and total organic matter, but it is not mature in the Hammerfest Basin.

The geological evolution of the Hammerfest Basin was first described in some detail by Bergland et al. (1986). During Late Palaeozoic to Late Jurassic times the area occupied by the present Hammerfest Basin was part of a regional intracratonic basin dominated by clastic deposition. This provided the preservation of Jurassic sequences which later were covered by Cretaceous and Tertiary sequences filling the basin. The Jurassic source rocks may have reached significant maturation in Mid Oligocene time when the area was subjected to significant uplift and subsequent erosion.

The severity and timing of Cenozoic exhumation in the southwestern Barents Sea was studied by Cavanagh et al. (2006). The juxtaposition of the North Atlantic rift system with the borderlands of the Eurasian Arctic shelf has resulted in a basin evolution in the southwestern Barents Sea. The erosion in the Hammerfest Basin is estimated to be in the range of 500–1500 m. However, the relative severity of individual episodes and impact on fluid dynamics within the basin are poorly constrained.

### **1.5. Objectives of the Study**

The main objective of this study is to understand the depositional evolution of the Hammerfest Basin and petroleum system through modelling two 2D seismic sections in the south western part of the Hammerfest basin

The specific objectives of the study are:

- To understand the influence of petroleum system on hydrocarbon maturity and generation from the source rocks and its effects to erosion and uplift.
- To determine the depositional evolution and subsidence history of the basin through modelling.
- To determine migration pathways and accumulation of the hydrocarbons of the petroleum system.

## Chapter 2

### 2.0 GEOLOGY OF THE STUDY AREA

#### 2.1. Regional Geology

In the western Barents Sea the Caledonian Orogeny involved the closure of the Iapetus Ocean, which had separated Eurasian from Laurentia. Deformation started during the Middle Ordovician, reaching a climax in the Silurian. The main arm of the Caledonides (the Barents Sea Caledonides) follows the general NE axis of the Scandinavian-Greenland Caledonides and is thought to underlie most of the southwestern Barents Sea and continue towards the NE (Gee et al. 2008). A separate northerly oriented arm, the Svalbard Caledonides, underlies the northwestern Barents Sea, and underwent a final Late Devonian compressive phase (Worsley, 2008).

Following the Caledonian Orogeny, Late Palaeozoic crustal extension led to the development of grabens and half grabens and, later, a regional sag basin covering major parts of the current Barents Shelf. Subsequent uplift to the east, induced by the onset of the Uralide Orogeny during the Devonian and Carboniferous-Permian plate collision (Ritzmann and Faleide 2009) led to a pronounced change in basin physiography in Late Palaeozoic to Early Triassic times. Post-Permian subsidence was primarily focused on the basins flanking Novaya Zemlya, and locally also in the Nordkapp Basin. To the west, the Hammerfest Basin formed as a post-Permian depocentre, separated by major faults from the Finnmark Platform and Loppa High.

A dominant feature of the Barents Sea stratigraphy is the major unconformity at the base of the Quaternary. Early Cretaceous strata sub-crop the unconformity from the eastern Hammerfest Basin to the Pechora Sea, and Jurassic-Triassic strata are truncated on major structural highs and across large areas of the shelf towards Svalbard. The unconformity is due to Palaeogene-Recent uplift and erosion of the entire Barents Sea to the east of the western margin (Henriksen et al. 2011), with erosion products being re-deposited to the west, particularly during the Late Pliocene-Pleistocene (Vorren et al. 1991).

A number of significant phases of basin development have occurred since the Emsian. Early rifting events include the first appearance of the Hammerfest Basin as a NE-trending half-graben during the Late Carboniferous (Oduro 1998; Hendriks 2003), widespread half-graben development and unroofing of the Loppa High during the Late Permian–Early Triassic (Hendriks and Andriessen

2002), and a failed plate break-up in the Late Jurassic–Early Cretaceous that separated deep basin development in the west from shallow platform areas in the east (Gabrielsen et al. 1997).

Oceanic crust developed along the entire continental margin from Norway to Svalbard during the Palaeogene, following Late Palaeocene rifting, as the Norwegian–Greenland Sea opened. The Sørvestnaget Basin records a thick and uninterrupted sequence of Palaeocene and Eocene sediments bounded to the west by the volcanic margin of the Senja Fracture Zone (Ryseth et al. 2003). The sequence is truncated as a result of shallow marine conditions during the Oligocene. Thick Neogene sedimentary wedges along the western edge of the passive margin (Nyland et al. 1992) and widespread indications of glacial grounding at the shelf edge testify to multiple ice sheet advances during the Pleistocene (Cavanagh et al 2006).

## **2.2. Lithostratigraphy of the Hammerfest Basin**

The lithostratigraphy of the Hammerfest Basin in southwestern Barents Sea is described by Dalland et al. (1988), Dallmann (1999) and Larssen et al. (2005). Moreover, NPD Bulletins no. 6 and 9 describe the lithostratigraphy of the Hammerfest Basin which is known from drilling and interpreted seismic sections to range from the Late Carboniferous to the Quaternary. Fig. 2.1 shows the lithostratigraphy of the Hammerfest Basin in the Barents Sea area.

The definitions of lithostratigraphical units are based mainly on well data from the Hammerfest Basin, but also taking into account data from the other structural provinces. Names presented are based on marine fauna of Norwegian waters together with coastal or offshore geographic names (Dalland et al., 1988).

PERIOD		NEO-GENE		PALEOGENE					CRETACEOUS					JURASSIC			TRIASSIC																											
GROUP	FORMATION	"T-UNIT"	FM	GP	MIO	P/P	EOC	OLI	Pal	Pal	Late	Early	Late	Mid	Early	Late	Late	Late	M	E	Age																							
							Chf	Rup	Prb	Lut	Ypr	Tha	Dan	Maa	Cmp	San	Cen	Alb	Apt	Brm	Hau	Vlg	Rya	Vol	Kim	Oxf	Civ	Bth	Bas	Aal	Toa	Pib	Sin	Het	Rht	Nor	Crn	Lad	Ans					
SOTBAKKEN	TORSK	T7		Egga																																								
					Loppa																																							
NY-GRUNNEN	KVEITE KVITING	T5		Kvaløy																																								
NORDVEST-BANKEN	KOLMULE	T4-4	Torsvåg																																									
	KOLJE	T4-2/3	Tamsøy/Anda																																									
	KNURR	T4-1	Slettnes																																									
TEISTEN-GRUNNEN	HEKKINGEN	T3-2	Olderfjord																																									
	FUGLEN	T3-1	Risfjord																																									
REALGRUNNEN	STØ	T2-5	Stø																																									
	NORDMELA	T2-4	Nordmela																																									
	TUBÅEN	T2-3	Dyrøy																																									
	FRUHOLMEN	T2-1/2	Ytterøy Heigøy																																									
INGØY-DJUPET	SNADD	T1-4	Aun																																									
	KOBBE	T1-3	Gimsøy																																									
	KLAPPMYS	T1-2	Andenes																																									
	HAVERT	T1-1	Svolvær																																									

Figure 2.1 Lithostratigraphy of the Hammerfest Basin with informal units (modified from Dalland et al. 1988).



## **2.3. Geological Evolution**

### **2.3.1. Carboniferous**

Development of fault-bounded basins commenced on Svalbard and Bjørnøya by the end of Devonian time (Steel & Worsley 1984) and on the Finnmark Platform during the Early Carboniferous (Bugge et al. 1995). The Barents Sea and Svalbard underwent further rifting during the Carboniferous (Worsley 2008). The rifts form a fan-shaped array of half-grabens and highs influenced by zones of weakness in the basement, coincident with Caledonian and older trends (Gudlaugsson et al. 1998). The tectonic phase is related to the initiation of the Atlantic rift system between Norway and Greenland in response to plate divergence and lithospheric stretching at the close of Devonian times. A major rift pulse is inferred for the Middle Carboniferous in the Atlantic rift and in the SW Barents Sea, with possible establishment of a structural connection to the Arctic rift (Gudlaugsson et al. 1998).

Several sedimentary basins (example, Tromsø, Bjørnøya, Nordkapp, Fingerdjupet, Maud and possibly Hammerfest) may have initiated at this time (Gudlaugsson et al. 1998). Basin development intensified in the Middle Carboniferous and fault-bounded subsidence and half-graben formation have been interpreted in both the southwestern Barents Sea and on the eastern Finnmark Platform (Gudlaugsson et al. 1998).

### **2.3.2. Late Carboniferous to Early Permian**

The central and eastern parts of the western Barents Sea experienced a shift to regional subsidence in the Late Carboniferous with development of a regional sag basin covering the entire Barents Shelf (Gudlaugsson et al. 1998). The regional sag was probably related to the closure of the Uralian Ocean along the eastern margin of Baltica.

A regional unconformity separates the Late Carboniferous–Early Permian strata from underlying rocks (Nilsen et al. 1993; Stemmerik 1997; Samuelsen et al. 2003; Stemmerik and Worsley 2005). Owing to continental drift the climate changed from humid tropical to sub-tropical and arid in the Late Carboniferous. Furthermore, from Bashkirian time, the continental post-Caledonian landscape in the western part of the Barents Shelf was transgressed and by Early Moscovian time warm water carbonate shelf conditions dominated most of the Barents–Pechora shelf (Smelror et al. 2009), with widespread evaporite deposition, both in the deep basins and in shallower salinas

and marginal sabkhas (Stemmerik 2000; Stemmerik&Worsley 2005). Continental conditions were presumably limited towards Fennoscandian land areas in the south and possibly also in the northern areas between Svalbard and Franz Joseph Land and in horst-like features along lineaments to the NW (Smelroret al. 2009).

### **2.3.3. Late Permian**

During the late Early Permian, the entire Barents Sea saw dramatic changes in the marine circulation systems, with development of a marine seaway between Norway and Greenland causing an abrupt change in oceanic circulation, as cool sea water flowed across the Barents Shelf (Stemmerik et al. 1999; Stemmerik and Worsley2005). During the Artinskian–Kungurian, the downdip parts of the highs were again transgressed and temperate water carbonates with bryozoan–Tubiphytes cement stone buildups formed (Stemmerik 1997). These were succeeded, however by cool water carbonates and spiculitic cherts of the Bjarmeland (Late Sakmarian–Kungurian) and Tempelfjorden (Kazanian–Tatarian) groups (Larssen et al. 2005).

### **2.3.4. Early–Late Triassic (Induan–Early Norian)**

Whereas the Uralide Orogen in Early Permian–Early Triassic times was dominated by thrusting of the East European Craton over the Siberian Craton, the final phase of deformation took place in Novaya Zemlya and to the east of Timan–Pechora, involving folding during Late Triassic–Early Jurassic times (Ritzmann and Faleide 2009). Rapid subsidence of the North and South Barents basins took place during the Late Permian and continued through the Triassic, with deposition of approximately 4–7 km of Triassic strata (Ritzmann and Faleide 2009).

The Triassic was tectonically a quiet period in the western Barents Sea with passive regional subsidence, but minor movements are observed on the Bjarmeland and Finnmark platforms. More active faults are found along the western margin, where the Loppa High was uplifted and eroded in the Early Triassic. However, stratal patterns across the Loppa High show that it subsequently became a significant depocentre in the Late Triassic before it was re-activated as a high in the Late Jurassic; it has apparently undergone several phases of inversion (Gabrielsen et al. 1993).

In the Nordkapp Basin halokinetic movement of the Late Palaeozoic salt was initiated in Early Triassic times and was followed by a series of shorter growth phases throughout Triassic time

(Nilsen et al. 1995). In the Maud Basin the salt movements started in Ladinian time, with the main diapiric phase in Late Cretaceous.

The Permian–Triassic boundary forms a regional unconformity in the Barents region. On Svalbard, subaerial exposure and weathering at the top of the Permian has been documented by Mørk et al. (1999a), with corroded Late Permian cherts overlain by Early Triassic sandstones and similar contacts have been seen on Edgeøya (Mørk et al. 1982) and on Bjørnøya (Mørk et al. 1990). On the offshore Svalis Dome the two basal Triassic ammonite zones are missing from Induan mudrocks on-lapping Late Permian bioclastic limestones (Vigran et al. 1998; Mørk&Elvebakk 1999). Bugge et al. (1995) also documented a limited stratigraphic break at the top of the Permian succession on the Finnmark Platform, where the uppermost Permian is partly eroded below Early Triassic marine mudrocks.

Across the Norwegian sector, the Induan–Early Norian succession shows a total thickness in excess of 2500 m, with four lithostratigraphic formations (in ascending order: Havert, Klappmyss, Kobbe and Snadd). Each of these can be related to regional regressive–transgressive cycles, with the formation boundaries picked at inferred maximum flooding events. As such they can be seen as genetic stratigraphic units (Galloway 1989). Reservoir rocks are generally present at the approximate levels of maximum regression, whereas petroleum source rocks are associated with marine anoxia during periods of maximum flooding and/or condensation. Biostratigraphic data yield the following ages for these main flooding events:

- Early Norian – Top of Snadd Formation;
- Late Anisian–Early Ladinian (Illyrian–Fassanian) – Top of Kobbe Formation;
- Late Olenekian–Early Anisian (Spathian–Aegian) – Top of Klappmyss Formation;
- Olenekian (Smithian) – Top of Havert Formation;
- Early Induan (Griesbachian) – Base of Havert Formation.

### **2.3.5. Late Triassic–Middle Jurassic**

The Late Triassic–Middle Jurassic (Early Norian–Bajocian) succession in the western Barents Sea embraces the main reservoirs in the Norwegian sector and includes four formations (Fruholmen, Tubaen, Nordmela and Stø) currently grouped into the Realgrunnen Subgroup of the Kapp Toscana Group (Dalland et al. 1988; Mørk et al. 1999b). The strata are bounded by the Early

Norian transgressive event at the basal contact with the Snadd Formation and by a regional Middle Jurassic unconformity/ condensed section below marine mudrocks in the overlying Fuglen Formation (Worsley 2008). Other notable unconformities are identified at the Rhaetian–Hettangian transition (base of the Tubaen Formation) and in the Early Toarcian (base of Stø Formation). In comparison, the time-equivalent succession in the South Barents Basin is stratigraphically more complete.

The Early Jurassic palaeogeographic setting was probably inherited from the Triassic. Shoreline regression followed after the Early Norian flooding, with the establishment of widespread deltaic and eventually alluvial systems in the Early Jurassic. A regional regressive maximum was reached during Hettangian–Sinemurian times, and the following phases of Early–Middle Jurassic deposition were dominated by regional transgression and gradual landwards translation of the shorelines (Henriksen et al., 2011a).

#### **2.3.6. Late Jurassic–Early Cretaceous**

Increasing tectonic activity through the Late Jurassic in the western Barents Sea culminated in the Early Cretaceous with the establishment of the present day structural configuration of basins and highs (Gabrielsen et al. 1990). The main rifting in the Barents Sea was restricted to the western basins, including the Hammerfest Basin, which subsided relative to the Loppa High and Finnmark Platform. Early Cretaceous tectonic subsidence along the western margin resulted in deposition of extremely thick Cretaceous successions in the Harstad, Tromsø, Bjørnøya and Sørvestsnaget basins (Faleide et al. 1993; Breivik et al. 1998).

To the north (Svalbard), progradation of Early Cretaceous fluvial and deltaic systems in the Helvetiafjellet Formation occurred (Gjelberg and Steel 1995). Furthermore, large-scale clinofolds prograding from the north in Lower Cretaceous strata are evident on seismic data. These events can be related to increased heat flow and uplift induced by rifting and eventual breakup and seafloor spreading associated with the opening of the Arctic Basin (Worsley 2008). This was accompanied by rather extensive magmatism, with emplacement of doleritic intrusions mainly into Triassic–Early Cretaceous shales; extrusive lavas are also present on Kong Karl Land and Franz Joseph Land (Gjelberg and Steel 1995). By Late Cretaceous the whole northern shelf margin was uplifted (Worsley 2008).

### **2.3.7. Late Cretaceous**

Significant subsidence persisted through the Late Cretaceous along the western margin and thick Late Cretaceous strata are present for instance in the Tromsø and Sørvestsnaget basins, where thicknesses exceeding 2 km can be inferred from seismic data. However, these strata are generally truncated to the east, below Cenozoic and Quaternary unconformities.

Where present, the strata comprise marine mudrocks deposited in an apparently well-oxygenated oceanic environment characteristic for the Late Cretaceous in the North Atlantic rift system. Although submarine fan systems of Santonian–Maastrichtian age exist further to the south (Vøring Basin: Lien et al. 2006), no such reservoir potential has so far been demonstrated for the Barents Sea margin.

Apparently, the oceanic depositional setting did not favour deposition of hydrocarbon source rocks. However, the potential existence of such deposits cannot be ruled out, as anoxic events have been recorded from the Sverdrup Basin (Leith et al. 1993) and from the Atlantic rift system as far north as the mid-Norway shelf (Cenomanian–Turonian; Dore´ et al. 1997).

### **2.3.8. Cenozoic**

Cenozoic evolution in the Barents Sea and particularly on its western margin is closely tied to the opening of the Norwegian–Greenland Sea, with significant shearing along the Senja Fracture Zone (ocean–continent boundary) as the spreading ridge propagated northwards, eventually forming a passive margin in the Oligocene (Nøttvedt et al. 1988; Faleide et al. 1996; Ryseth et al. 2003). Seafloor spreading began in the Norwegian–Greenland Sea by magnetic Anomaly 24 (Early Eocene). Significant reorganization of the spreading patterns occurred at Anomaly 21 (Middle Eocene), when spreading extended as far north as the southern limit of the Hornsund Fault Zone, and also at Anomaly 13 (Early Oligocene).

A dextral stress field was set up along the Senja–Hornsund alignment. Tectonic compression along this fault zone, between Svalbard and north Greenland, is expressed by the fold-and-thrust belt on Svalbard (Steel et al. 1985). Widespread inversion and compression features are found throughout the Barents Sea. Dore´ & Lundin (1996) noted that Cenozoic phases of compression and inversion are common within the NE Atlantic realm, with important phases of structuring occurring during the Oligocene and Miocene. These phases may relate to the plate tectonic changes in the NE

Atlantic, as well as to major Alpine deformation phases. Accordingly it seems reasonable to favour an Oligocene–Miocene age for many of the inversion structures in the Barents Sea.

Cenozoic strata are present over large areas of the western Barents Sea, but are less widespread than the underlying Cretaceous and older units. Palaeocene–Early Eocene marine mudrocks are generally present in the Hammerfest Basin and western part of the Nordkapp Basin, resting unconformably on the Cretaceous with a marked depositional break (Gabrielsen et al. 1990; Faleide et al. 1993). However, Cenozoic strata are absent (eroded) below the base of the Quaternary in surrounding platform areas such as the Finnmark and Bjarmeland platforms and parts of the Loppa High (Gabrielsen et al. 1990) and also generally in the northern part of the Barents Sea (Grogan et al. 1999). Further east, significant uplift in the South Barents Basin can also be inferred from the observed truncation of Cretaceous strata below the Quaternary. Accordingly, the limited distribution of Cenozoic strata is due to uplift and subsequent glacial erosion to the east, accompanied by contemporary subsidence along the western margin, with re-deposition of eroded material and formation of a thick glacial wedge during the Late Pliocene–Pleistocene (Vorren et al. 1991; Eidvin et al. 1993; Richardsen et al. 1993; Faleide et al. 1996; Henriksen et al. 2011).

## Chapter 3

### 3.0 HAMMERFEST BASIN PLAYS

A play is a geographically and stratigraphically delimited area where a specific set of geological factors such as reservoir rock, trap, mature source rock and migration paths exist in order that petroleum may be provable (NPD definition). There are seven plays in Barents Sea area in which three of them are located in the Hammerfest Basin (Rodrigues Duran et al., 2013 and NPD). These three plays include Upper Jurassic to Lower Cretaceous plays, Lower to Middle Jurassic plays and Triassic plays. The geological factors (such as source rocks, reservoir rocks, seal/cap rocks and traps) of the Hammerfest Basin plays are described below:

#### 3.1. Hydrocarbon Source Rocks

##### 3.1.1. Hekkingen Formation

The organic rich shales/claystones of the Hekkingen Formation were deposited during Kimmeridgian to Early Cretaceous (pre-Valanginian). This sequence which probably consists of several different hydrocarbon source rock facies, is equivalent to the Spekk Formation, the Draupne Formation of the more southerly areas of the Norwegian Shelf. In the Hammerfest Basin this facies show hydrogen indices of up to 500 and oxygen indices of less than 20. The kerogen input appears to be basically type II with an influx of type III in the very south western part of the basin (Ohm et al., 2008). The terrestrial kerogen influx in this area is probably derived from the Finnmark Platform. It is believed that the Hekkingen Formation contains the most important source rocks in the Hammerfest Basin (Dalland et al., 1988).

##### 3.1.2. Snadd Formation

According to Berglund (1986) the Snadd Formation was deposited in a marginal marine to fluvial environment during Norian to Rhaetian times. The lithology of the sequence consists of interbedded claystones, shales and siltstones, sandstones and thin coals. The shales and claystones occasionally feature hydrogen indices in excess of 300 in a relatively proximal position to the Troms-Finnmark Fault Complex. The sediments do not appear to be buried deep enough to generate gas in the south eastern part of the basin. Shales in the Snadd Formation, however, have been a gas source in the western parts of the basin.

### **3.1.3. Kobbe Formation**

The Kobbe Formation was deposited during Early Carnian times as a mixed shale/claystone/siltstone sequence. The facies is a part of a delta prograding across the basin from the south east towards the north west. In the south eastern part of the basin this sequence contains a type III kerogen capable of generating gas and probably some condensate when subjected to sufficiently high temperatures. This interval is the source rock of the gas encountered in this part of the basin. The thickening of the delta towards the centre of the basin, in conjunction with an increased terrestrial kerogen input to the sediments, may result in this source rock sequence losing its richness and importance as a hydrocarbon source (Berglund et al., 1986).

## **3.2. Reservoir Rocks**

### **3.2.1. Sto Formation**

The Stø Formation overlies the Nordmela Formation with a sharp contact, often defined by a conglomeratic lag at the base of a thick sandstone unit. The formation consists mainly of fine to medium grained sandstones in the lower part with intervals of large scale cross stratification. Very fine to fine highly bioturbated sands dominate in the upper part which also includes up to three thin mudstone beds. Thin intervals with pebbly sandstones are present within the upper part. Phosphorite nodules are locally present in the upper most part of the formation. The Sto Formation represents, in general shoreline and near shore depositional environments strongly influenced by storm wave processes and bioturbation. Certain intervals in the lower part also seem to have some tidal influence, though, relatively strong unidirectional currents mainly dominated (Dalland et al. 1988).

### **3.2.2. Tubaen Formation**

The Tubaen Formation appears to be laterally extensive and varies in thickness from some 50 m to more than 130 m. In the western part of the explored area the upper part of the formation shows prominent upward coarsening and is interpreted as prograding mouth delta front sands with a lateral fluvial equivalent. The rest of the formation is generally thought to be of upper delta plain origin, dominated by meandering channels. The reservoir potential of the formation is well known and it has significance due to its thickness and wide distribution (Berglund et al., 1986).



### **3.3. Seals/Cap Rocks**

The cap rock of basin-centered traps is commonly thicker and has better sealing capacity than at the rim of the basin, which also tends to be more faulted (Ohm et al., 2008). Thus, distal basin peripheral traps in uplifted areas have a higher chance of containing oil because their cap rock may be partially leaking, allowing gas to bleed off while retaining oil (Sales, 1993).

#### **3.3.1. Fuglen Formation**

The Fuglen Formation was deposited during the Late Callovian to Oxfordian. The Formation was deposited in a marine environment during a highstand with ongoing tectonic movements. The formation is thickest in south west parts of the Hammerfest Basin, thinning to less than 10 m on the central highs in the basin, these areas are characterized by rare, thin limestone and by pyritic shales. It forms a potential cap/seal rock in the area (Dalland et al. 1988).

#### **3.3.2. Hekkingen Formation**

The organic rich shales/claystones of the Hekkingen Formation were deposited during Late Jurassic to Early Cretaceous. It is believed to be the main seal in the Hammerfest Basin region (Cavanagh et al., 2006). The lower boundary of Hekkingen Formation is defined by the transition from carbonate cemented and pyritic mudstone to poorly consolidated shale in the Fuglen Formation. The upper boundary in the reference well (7120/12-1) is defined towards the thin sandy limestone of the Knurr Formation. The dominant lithology in the formation is shale and mudstone with occasional thin interbeds of limestone, dolomite, siltstone and sandstone. The amount of sandstone increases towards the basin margins. The formation was deposited in a deep shelf with partly anoxic conditions (Norwegian Petroleum Directorate).

### **3.4. Traps**

A trap is a configuration of rocks suitable for containing hydrocarbons and sealed by a relatively impermeable formation through which hydrocarbons will not migrate. Traps can be structural (such as folds and faults) or stratigraphic traps (such as unconformities, pinch out and reefs). The Hammerfest Basin plays consist of both structural traps and stratigraphic traps which make the accumulation of the hydrocarbons possible. Upper Jurassic to Lower Cretaceous plays contains stratigraphic pinch-out traps and fault dependent traps. Lower to Middle Jurassic plays comprises of rotated fault blocks and horst structures traps and Triassic plays contains mainly stratigraphic traps and rotated fault blocks and halokinetic as structural traps (NPD).

# Chapter 4

## 4.0 METHODOLOGY

The basin modelling conducted in this study is based on two seismic lines BSS01-104 and BSS01-106. These two lines come from regional seismic lines BSS01-104\_FM\_TVFGC and BSS01-106\_FM\_TVFGC as shown on Fig 4.1. The sections were first interpreted using Schlumberger Petrel Software. After interpretation and depth conversion of these two sections, they were imported to the PetroMod software for basin modelling. To complete the study the following procedures were used;

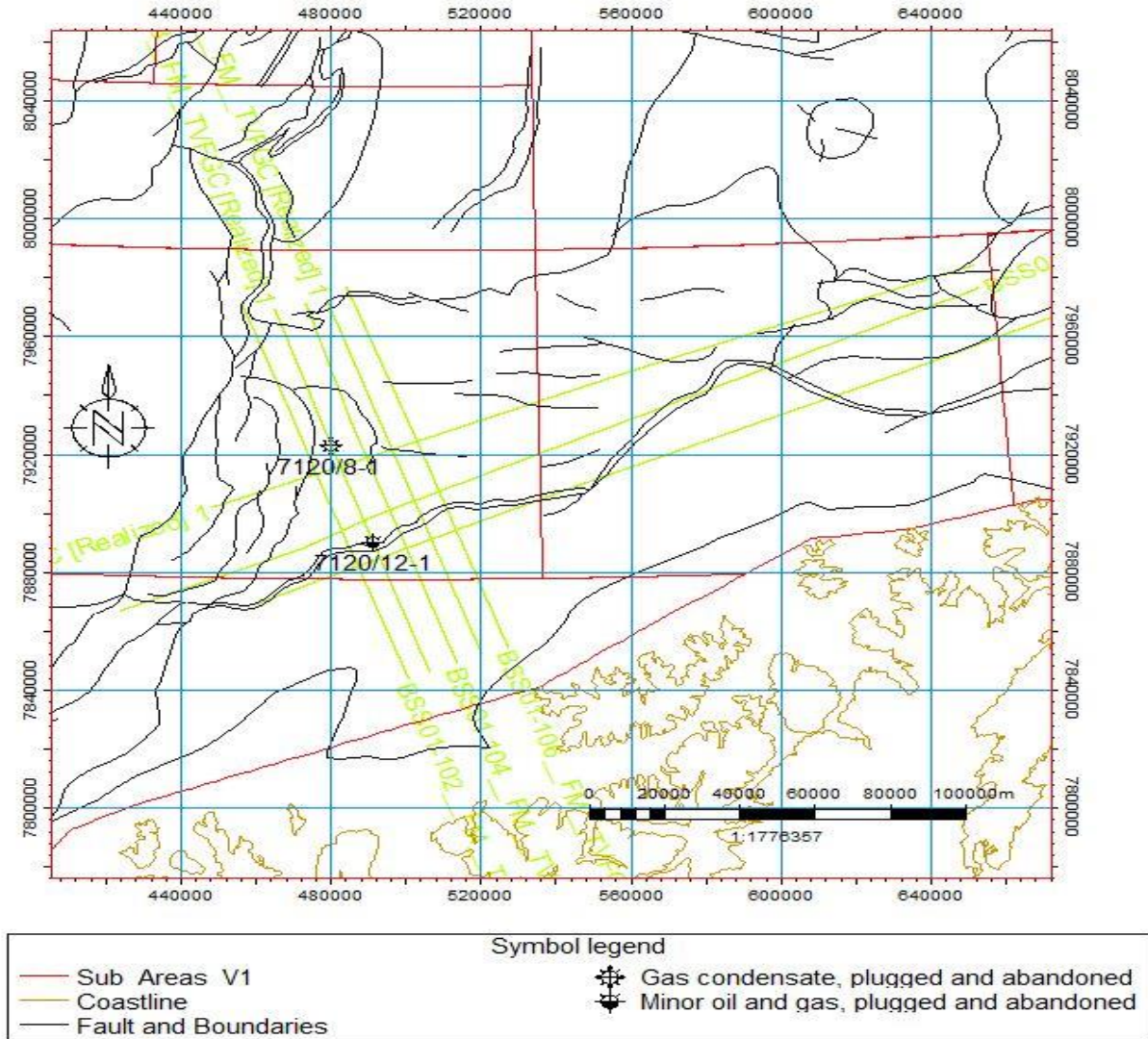


Figure 4.1 2D seismic lines BSS01-104 and BSS01-106 used in basin modelling.

#### 4.1. Data Compilation

Compilation of the data involves the mapping and gridding of the seismic lines together with well data and is a time consuming step. The data was interpreted in time domain, followed by velocity model creation and finally changed to depth domain for modeling purpose.

#### 4.2. Velocity Model Creation

In order to map out the thickness and depth of the subsurface layers, a seismic model creation is an essential process to be conducted in the interpreted seismic section. The following procedures were followed to create a seismic velocity model in this study. The interval velocity for each package was taken from the synthetic seismogram and the surface maps created were used to create the velocity modelling. Moreover, the average value was used to represent packages with more velocity values. The parameters used to create velocity model are shown in Fig. 4.2 and Table 4.1.

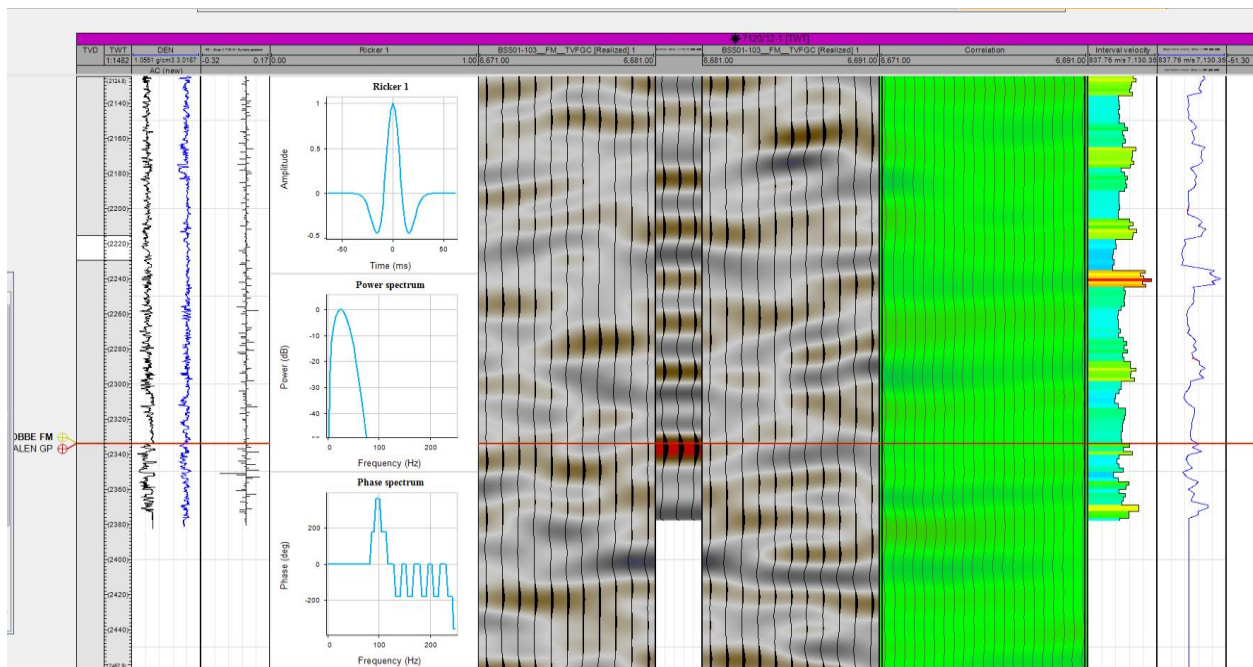


Figure 4.2 Synthetic generation window showing interval velocity of the interpreted horizons, which are used for velocity model creation.

Table 4.1 Parameters used to create the velocity model.

Make velocity model Hints

Create new: Velocity model

Edit existing: Velocity model (TWT to Z or back)

Convert from: TWT to: Z or back.

Datum

Time: SRD

Other:

Apply filter: Saved searches


	Base		Correction		Model	
	Surface		Sea be	Well tops		NORDL V=V0=VInt V0: Constant 1362
	Surface		Surface	Well tops		TORSK V=V0=VInt V0: Constant 2117
	Surface		Surface	Well tops		KVEITE V=V0=VInt V0: Constant 1994
	Surface		Surface	Well tops		KOLMU V=V0=VInt V0: Constant 2341
	Surface		Surface	Well tops		KOLJE V=V0=VInt V0: Constant 2358
	Surface		Surface	Well tops		KNURR V=V0=VInt V0: Constant 2755
	Surface		Surface	Well tops		HEKKI V=V0=VInt V0: Constant 3349
	Surface		Surface	Well tops		STØ F V=V0=VInt V0: Constant 4356
	Surface		Surface	Well tops		NORD V=V0=VInt V0: Constant 4631
	Surface		Surface	Well tops		TUBÅE V=V0=VInt V0: Constant 3420
	Surface		Surface	Well tops		FRUHO V=V0=VInt V0: Constant 4401
	Surface		Surface	Well tops		SNADD V=V0=VInt V0: Constant 4209
	Surface		Surface	Well tops		KOBBE V=V0=VInt V0: Constant 4687

### 4.3. Time to Depth Conversion

It is important to convert time to depth domain of the seismic section because it eliminates the structural uncertainty involved with time and confirms the structure at certain depth. The geological structure in seismic sections is interpreted when it is in the form of time domain. During geological model creation the time domain of the interpreted section have to be converted to depth domain (true vertical depth) by using a velocity model. The converted seismic line is then loaded to PetroMod software for the 2D modelling. Table 4.2 shows the depth converted lines.



Table 4.2 Depth converted seismic lines which can be used for 2D modelling.

Depth convert				
Velocity model:  Velocity model (TWT to Z or back)				
	Domain	Object	Direction	Interpolation
1	Seismic	BSS01-103__FM__	TWT -> Z	Smooth
2	Seismic	BSS01-104__FM__	TWT -> Z	Smooth
3	Seismic	BSS01-105__FM__	TWT -> Z	Smooth
4	Seismic	BSS01-102__FM__	TWT -> Z	Smooth
5	Seismic	BSS01-106__FM__	TWT -> Z	Smooth

#### 4.4. Interpreted Seismic Section reflectors Observation

The horizons and faults of seismic sections were interpreted based on the quality and configuration of the reflectors and depth converted for modelling of the petroleum systems. The PetroMod software was used for modelling the sections. It is crucial to convert the section from time to depth domain because PetroMod software accepts the section which is in depth domain for modelling. Fig. 4.3 show the reflectors of interpreted section 104 and two wells located at the section.

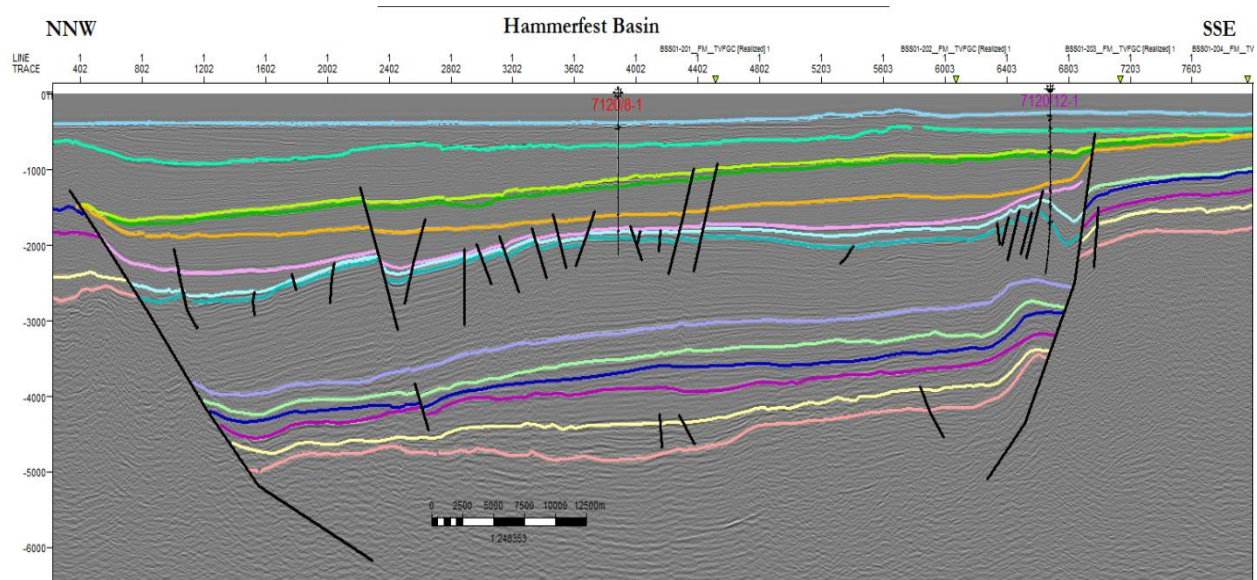

















Figure 4.3 Depth converted seismic section BSS01-104 and two wells located at the section.

## Legend

	Lower Carboniferous		Intra Lower Cretaceous (Hauterivian)
	Near Base of Permian		Intra Lower Cretaceous (Barremian)
	Near Top of Permian		Intra Lower Cretaceous
	Intra Lower Triassic		Upper Cretaceous
	Base of Middle Triassic		Base Tertiary
	Intra Upper Triassic		Base of Quaternary
	Base of Upper Jurassic		Top Nordland Gp (Sea bed)
	Faults		

In general the reflectors on the seismic section differ in configuration, amplitude and continuity, the observed reflectors show the following characteristics:

The Lower Carboniferous reflector/horizon is a low to medium amplitude continuous reflector. It is cross cut by two major faults on both sides of the sections. The downward movement of the blocks triggers the formation of the hanging wall in the center of the basin (Fig. 4.3).

Near Base of Permian is a moderate to high amplitude reflector which is characterized by high frequency and continuous faulted reflector. It is also bounded by the major faults as the Lower Carboniferous reflector (Fig. 4.3).

The Near Top of Permian is marked by a continuous and high amplitude reflector. It overlies the Near Base of Permian package which is also forms wedge shape due to tectonic activities.

The Intra Lower Triassic reflector is a continuous and moderate to high amplitude reflector. The package overlying the Intra Lower Triassic reflector has parallel and uniform thickness with the package beneath (Fig. 4.3).

The Base Middle Triassic and Intra Upper Triassic reflectors both are bounded by major faults and characterized with medium to high amplitude and continuous reflectors. The packages form wedge shapes which are thinning away from the faults (Fig. 4.3).

The reflector of Base Upper Jurassic is characterized by medium amplitude and continuous reflector which is bounded by major faults. The stage of rift formation can be observed in this package. The wedge shape formation near the major faults is evidence of the syn-rift event (Fig. 4.3).

Intra Lower Cretaceous 1, 2 and 3 reflectors are highly affected by faults and marked by medium to high amplitude and continuous reflectors. The rotated faulted blocks and discontinuous faults was observed in these packages. The upward movement of the package near to major faults indicates the compressional force from the surrounding blocks (Fig. 4.3).

Base Tertiary, Base Quaternary and the Sea bed reflectors are not affected by the major faults and characterized by high amplitude, sub parallel horizontal continuous reflectors. These reflectors are affected by truncation erosion in southeastern part and dip towards the northwestern part of the section. These reflector packages forms the post-rift packages of the Hammerfest Basin which is characterized by onlap surface and unconformity above the Base Quaternary (BQ) reflector (Fig. 4.3).

## Chapter 5

### 5.0 2D BASIN MODELLING

#### 5.1. Software

2D petroleum system models were built by using 2D PetroBuilder in PetroMod Software. The depositional evolution of sedimentary basin has been modelled in PetroMod software by input information such as layers/strata, define facies and boundary conditions. This allows estimating whether hydrocarbons have filled the reservoir or not, the source rock maturation and generation of hydrocarbons, amount of hydrocarbons present at the reservoir, formation of the trap, migration of the hydrocarbons and hydrocarbon types.

Fig .5.1 shows the basic model building process, which includes:

- Load interpreted image and digitization of horizons and faults.
- Fault properties assignment.
- Age and layers assignment.
- Layer splitting and processing.
- Facies definition assignment.
- Assign boundary conditions such as; paleo water depth (PWD), sediment water interface temperature (SWIT) and heat flow (HF).
- Setting the simulator options and parameters.



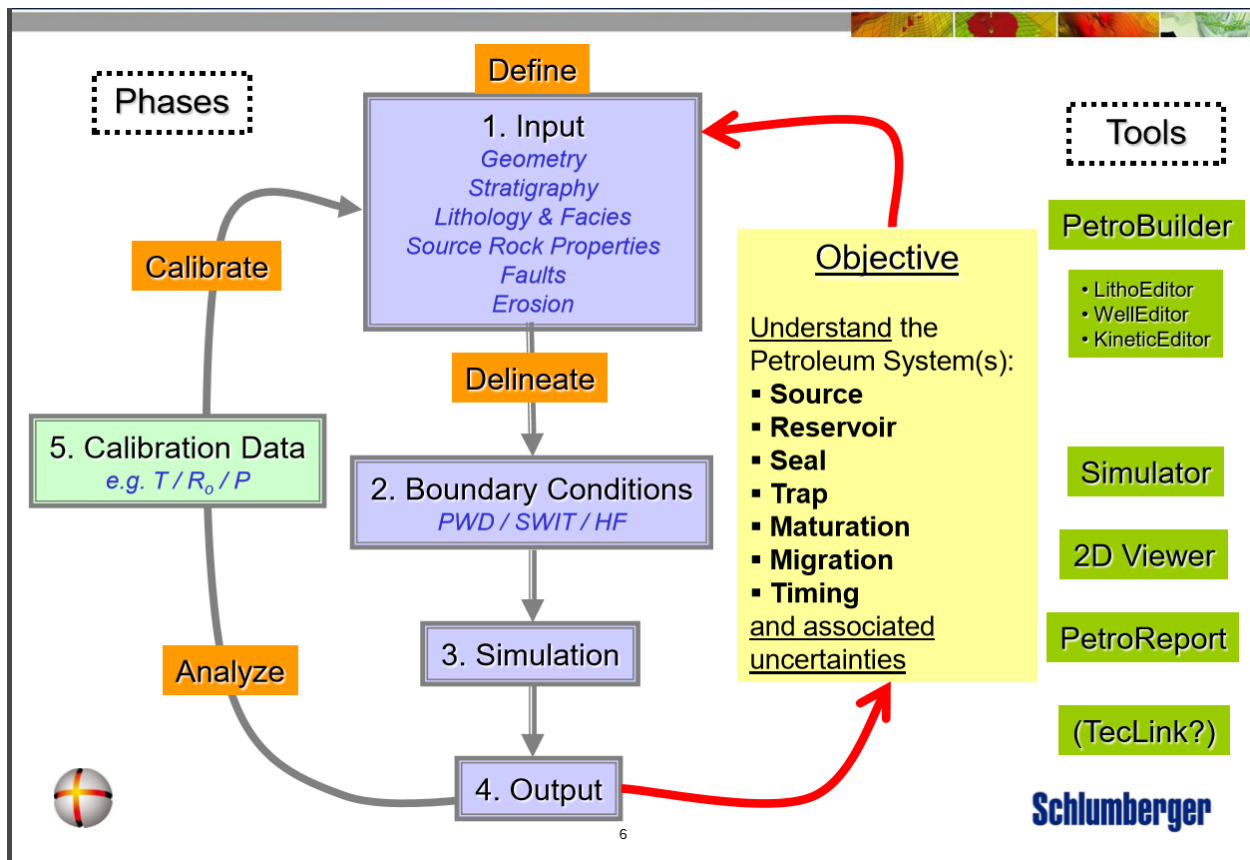
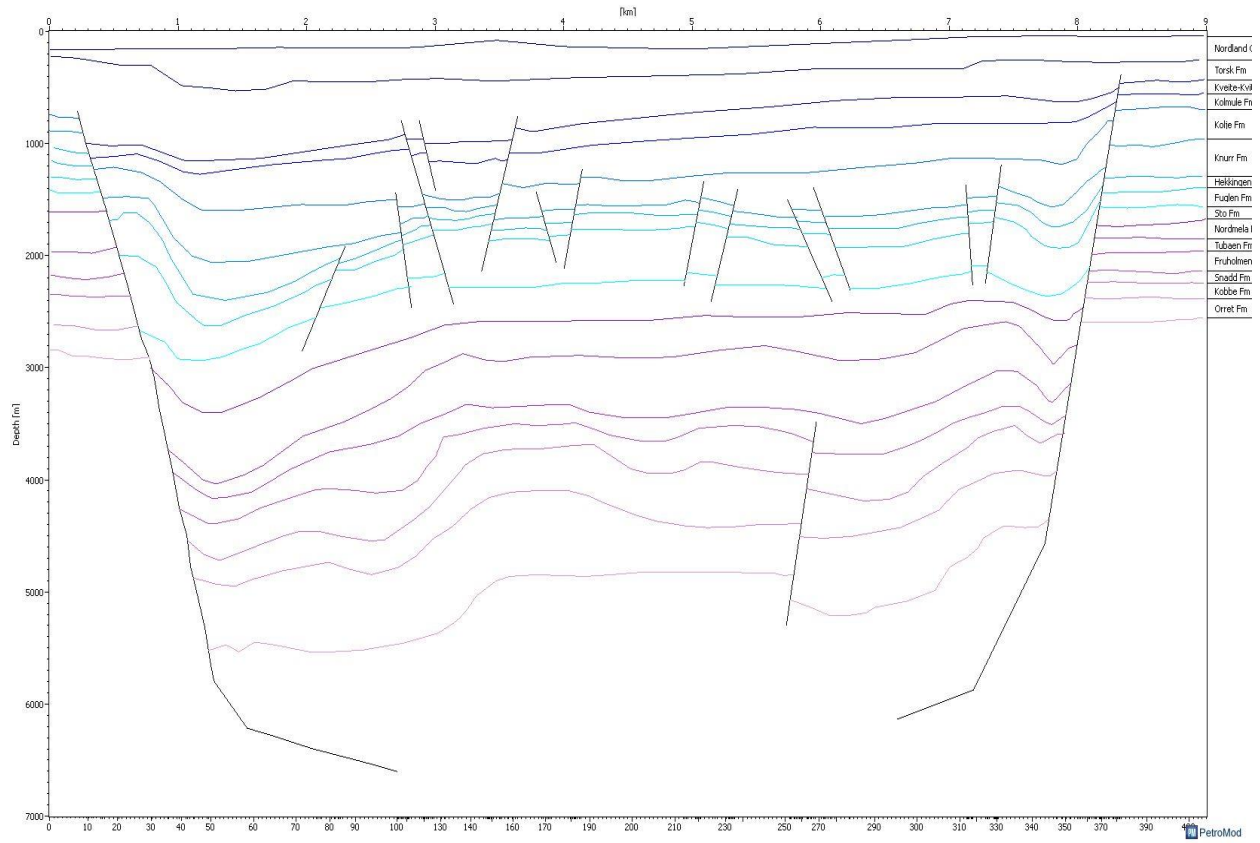


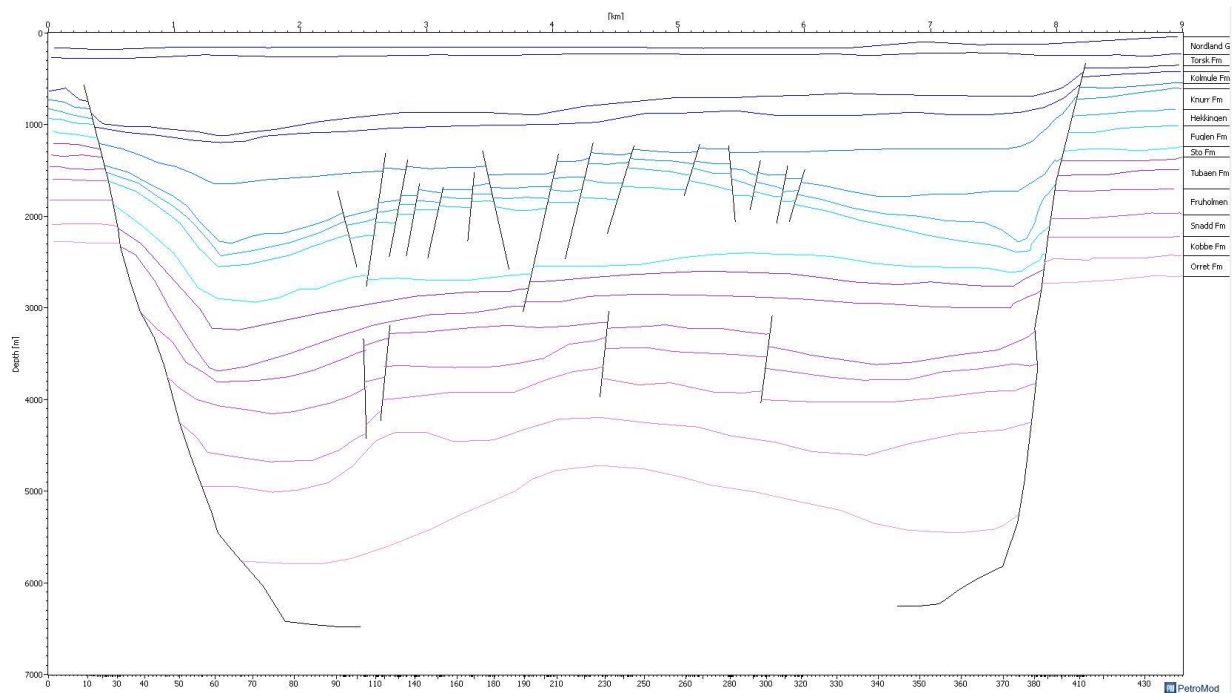
Figure 5.1 2D Modelling workflow.

## 5.2. Data Input

Norwegian Petroleum Directorate (NPD) fact pages and primary information from the literature were used for modelling. The depth converted seismic lines from Petrel software was directly imported in PetroMod software for 2D basin modelling. To confirm the horizon and fault intersect on grid point and reach the boundary of the model, the gridding of the pre-grid horizons and pre-grid faults was done. The digitization of the interpreted horizons and faults was done by using PetroMod software manually. The fault model was created on completion of the digitization process, followed by gridding process. The section is ready for model development after completion of the digitization, fault model creation and gridding of the faults and horizons process confirmed. Figs. 5.2 and 5.3 show the pre-grid model view of the digitized horizons and faults.



*Figure 5.2 Pre-grid model view of the digitized horizons and faults and layer splitting for model line 104 (In interpreted section only 13 layers can be seen, due to layer splitting 16 layers can be seen in this figure)*



*Figure 5.3 Pre-grid model view of the digitized horizons and faults and layer splitting for model 106 (In interpreted section only 13 layers can be seen, due to layer splitting 16 layers can be seen in this figure)*

### **5.3. Fault Properties Definition**

The properties such as period, age and type of the faults can be defined in the PetroMod software. The faults were assigned to the PetroMod software for modelling. Total of sixteen interpreted faults have been assigned for model 104 and twenty two interpreted faults have been assigned for model 106. The faults largely developed during the Late Jurassic to Early Cretaceous rifting event. Thus the age of the faults was assigned as Late Jurassic (145 Ma). However, faults can be open at different time intervals but it is considered Late Jurassic due to the major rifting events which took place at this time. During rifting the faults were possible open (non-sealing) or closed (sealing), all faults were assumed to be closed in model 104 and only two major faults in model 106 were assumed to be closed and remains faults in model 106 were all assumed to be open. This is because the sealing and non-sealing capacity of the faults has effects on the hydrocarbons migration and accumulations, thus the faults were assumed to be closed in model 104 and open in model 106 to observe this effects (Tables 5.1 and 5.2).

Table 5.1 Faults properties definition table for model 104.

Name	-	Period	Age from [Ma]	Age to [Ma]	Type
Fault_1		1	145.00	0.00	Closed
Fault_2		1	145.00	0.00	Closed
Fault_3		1	145.00	0.00	Closed
Fault_4		1	145.00	0.00	Closed
Fault_5		1	145.00	0.00	Closed
Fault_6		1	145.00	0.00	Closed
Fault_7		1	145.00	0.00	Closed
Fault_8		1	145.00	0.00	Closed
Fault_9		1	145.00	0.00	Closed
Fault_10		1	145.00	0.00	Closed
Fault_11		1	145.00	0.00	Closed
Fault_12		1	145.00	0.00	Closed
Fault_13		1	145.00	0.00	Closed
Fault_14		1	145.00	0.00	Closed
Fault_15		1	145.00	0.00	Closed
Fault_16		1	145.00	0.00	Closed

Table 5.2 Faults properties definition table for model 106

Name	-	Period	Age from [Ma]	Age to [Ma]	Type
Fault_1		1	145.00	0.00	Closed
Fault_2		1	145.00	0.00	Open
Fault_3		1	145.00	0.00	Closed
Fault_4		1	145.00	0.00	Open
Fault_5		1	145.00	0.00	Open
Fault_6		1	145.00	0.00	Open
Fault_7		1	145.00	0.00	Open
Fault_8		1	145.00	0.00	Open
Fault_9		1	145.00	0.00	Open
Fault_10		1	145.00	0.00	Open
Fault_11		1	145.00	0.00	Open
Fault_12		1	145.00	0.00	Open
Fault_13		1	145.00	0.00	Open
Fault_14		1	145.00	0.00	Open
Fault_15		1	145.00	0.00	Open
Fault_16		1	145.00	0.00	Open
Fault_17		1	145.00	0.00	Open
Fault_18		1	145.00	0.00	Open
Fault_19		1	145.00	0.00	Open
Fault_20		1	145.00	0.00	Open
Fault_21		1	145.00	0.00	Open
Fault_22		1	145.00	0.00	Open

#### 5.4. Age Assignment

The age information (Tables 5.3 and 5.4) was taken from Norwegian Petroleum Directorate Bulletin no. 4 and 6 and other published literature such as (Duran et al. 2013a and Ohm et al. 2008). Three major erosions were assigned to the age assignment table, Late Cretaceous erosion which eroded 200m of layer thickness, Base Paleocene erosion which eroded 300m of layer thickness and Base Quaternary erosion which eroded 500m of layer thickness. The oldest reflector is Lower Carboniferous, which is around 354 Ma and youngest reflector is the Top Nordland Group around 0.0 Ma. The thickness of the eroded layer was also estimated to be 1000 m in total

for all three phases of erosions. The amount and duration of erosion assigned in the table is based on Rodrigues Duran et al. (2013a).

Table 5.3 Age assignment table for model 104








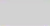






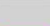










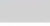


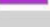






Age [Ma]	Horizon	-	Pre-grid Horizon	Gridded Horizon	Erosion Map	Layer	-	Event Type	Facies Map	No. of Sublayers	Max. Time Step [Ma]	
1	1.50	Nordland Gp.	 →	Horizon_1	→	Horizon_1_Map	→					
2						Nordland Gp.		Deposition	→	Map_Layer_1_Facies	1	10.00
3	53.50	Erosion_87_Top										
4						Erosion_87_Top		Erosion			10.00	
5	55.00	Torsk Fm.	 →	Horizon_2	→	Horizon_4_Map	→	ErosionMapID3_55				
6						Torsk Fm.		Deposition	→	Map_Layer_2_Facies	1	10.00
7	65.00	Erosion_89_Top										
8						Erosion_89_Top		Erosion			10.00	
9	74.00	Kveite-Kvitling Fms.	 →	Horizon_3	→	Horizon_5_Map	→	ErosionMapID1_74				
10						Kveite-Kvitling Fms.		Deposition	→	Map_Layer_3_Facies	1	10.00
11	99.00	Kolmule Fm.	 →	Horizon_4	→	Horizon_6_Map	→					
12						Kolmule Fm.		Deposition	→	Map_Layer_4_Facies	1	10.00
13	121.00	Kolje Fm.	 →	Horizon_5	→	Horizon_7_Map	→					
14						Kolje Fm.		Deposition	→	Map_Layer_5_Facies	1	10.00
15	125.00	Knurr Fm.	 →	Horizon_6	→	Horizon_8_Map	→					
16						Knurr Fm.		Deposition	→	Map_Layer_6_Facies	1	10.00
17	130.00	Hekkingen Fm.	 →	Horizon_7	→	Horizon_9_Map	→					
18						Hekkingen Fm.		Deposition	→	Map_Layer_7_Facies	1	10.00
19	160.00	Mid Jurassic	 →	Horizon_14	→	Horizon_10_Map	→					
20						Mid Jurassic		Deposition	→	Map_Layer_8_Facies	1	10.00
21	180.00	Fuglen Fm.	 →	Layer_8_1	→	Layer_8_1	→					
22						Fuglen Fm.		Deposition	→	Map_Layer_8_Facies_Split_1	1	10.00
23	242.00	Sto Fm.	 →	Layer_8_2	→	Layer_8_2	→					
24						Sto Fm.		Deposition	→	Map_Layer_8_Facies_Split_2	1	10.00
25	245.00	Nordmela Fm.	 →	Layer_8_3	→	Layer_8_3	→					
26						Nordmela Fm.		Deposition	→	Map_Layer_8_Facies_Split_3	1	10.00
27	260.00	Tubaen Fm.	 →	Horizon_8	→	Horizon_11_Map	→					
28						Tubaen Fm.		Deposition	→	Map_Layer_9_Facies	1	10.00
29	270.00	Fruholmen Fm.	 →	Horizon_9	→	Horizon_12_Map	→					
30						Fruholmen Fm.		Deposition	→	Map_Layer_10_Facies	1	10.00
31	290.00	Snadd Fm.	 →	Horizon_10	→	Horizon_13_Map	→					
32						Snadd Fm.		Deposition	→	Map_Layer_11_Facies	1	10.00
33	300.00	Kobbe Fm.	 →	Horizon_11	→	Horizon_14_Map	→					
34						Kobbe Fm.		Deposition	→	Map_Layer_12_Facies	1	10.00
35	354.00	Orret Fm.	 →	Horizon_12	→	Horizon_15_Map	→					
36						Orret Fm.		Deposition	→	Map_Layer_13_Facies	1	10.00
37	400.00	Basement	 →	Horizon_13	→	Horizon_16_Map	→					



Table 5.4 Age assignment table for model 106

	Age [Ma]	Horizon	-	Pre-grid Horizon	Gridded Horizon	Erosion Map	Layer	-	Event Type	Facies Map	No. of Sublayers	Max. Time Step [Ma]
1	0.00	Nordland Gp top		Horizon_1	Horizon_1_Map							
2							Nordlan...		Deposition	Map_Layer_1_Facies	1	10.00
3	54.00	Erosion_46_Top										
4							Erosion_...		Erosion			10.00
5	55.00	Torsk Fm		Horizon_2	Horizon_3_Map	ErosionMapID1_55						
6							Torsk Fm		Deposition	Map_Layer_2_Facies	1	10.00
7	65.00	Erosion_54_Top										
8							Erosion_...		Erosion			10.00
9	74.00	Kveite-Kviting		Horizon_3	Horizon_4_Map	ErosionMapID2_74						
10							Kveite-K...		Deposition	Map_Layer_3_Facies	1	10.00
11	99.00	Kolmule Fm		Horizon_4	Horizon_5_Map							
12							Kolmule ...		Deposition	Map_Layer_4_Facies	1	10.00
13	121...	Kolje Fm		Horizon_5	Horizon_6_Map							
14							Kolje Fm		Deposition	Map_Layer_5_Facies	1	10.00
15	125...	Knurr Fm		Horizon_6	Horizon_7_Map							
16							Knurr Fm		Deposition	Map_Layer_6_Facies	1	10.00
17	130...	Hekkingen Fm		Horizon_7	Horizon_8_Map							
18							Hekking...		Deposition	Map_Layer_7_Facies	1	10.00
19	160...	Fuglen Fm		Horizon_8	Horizon_9_Map							
20							Fuglen Fm		Deposition	Map_Layer_8_Facies	1	10.00
21	180...	Sto Fm		Horizon_9	Horizon_10_Map							
22							Sto Fm		Deposition	Map_Layer_9_Facies	1	10.00
23	242...	Nordmela Fm		Horizon_10	Horizon_11_Map							
24							Nordmel...		Deposition	Map_Layer_10_Facies	1	10.00
25	245...	Tubaen Fm		Horizon_13	Horizon_12_Map							
26							Tubaen ...		Deposition	Map_Layer_11_Facies	1	10.00
27	260...	Fruholmen Fm		Horizon_11	Horizon_13_Map							
28							Fruholm...		Deposition	Map_Layer_12_Facies	1	10.00
29	270...	Snadd Fm		Horizon_12	Horizon_14_Map							
30							Snadd Fm		Deposition	Map_Layer_13_Facies	1	10.00
31	290...	Kobbe Fm		Horizon_14	Horizon_15_Map							
32							Kobbe Fm		Deposition	Map_Layer_14_Facies	1	10.00
33	300...	Orret Fm		Horizon_15	Horizon_16_Map							
34							Orret Fm		Deposition	Map_Layer_15_Facies	1	10.00
35	354...	Basement		Horizon_16	Horizon_17_Map							

## 5.5. Facies Definition

Tables 5.5 and 5.6 define the facies and characteristics of the different layers used in the model. The Snadd, Kobbe Formation and Hekkingen Formations are defined as the source rocks. Properties such as Hydrogen Index (HI), Total Organic Carbon (TOC) and Kinetics of the source rock were assigned to the facies definition table. According to Ohm et al. (2008) the shale TOC contents for the Kobbe, Snadd and Hekkingen Formations are around 3-5%, 2-4% and 8-12% respectively. In addition to that the Hydrogen Index is 200mg/gTOC, 150mg/gTOC and

300mg/gTOC and the Kerogene types are TIII, TIII and TII-TIII respectively. The values of TOC and HI were assigned in the model for each source rock as mentioned above. The reaction kinetics used is Burnham (1989) \_TII and Burnham (1989) \_TIII because the Hekkingen Formation is the type II-type III source rock and Snadd and Kobbe Formations are type III source rocks.

The Sto and Tubaen Formations were defined as the reservoir rock whereas the Fuglen Formation was defined as the seal rock. The study done by Berglund et al. (1986) shows that most hydrocarbons in the Hammerfest Basin are preserved in Middle Jurassic Sto and Tubaen sandstones. The remaining layers were defined as the overburden and underburden rocks.

Table 5.5 Facies definition table for model 104








































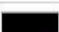




























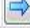





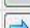


















Name	Color	Lithology Value	TOC Mode	TOC Value [%]	TOC Map	Kinetics	HI Mode	HI Value [mgHC/gTOC]	HI Map	Petroleum System Elements
Nordland Gp.		Siltstone (organic lean)								Overburden Rock
Torsk Fm.		Shale (organic lean, typical)								Overburden Rock
Kveite-Kviting Fm.		Siltstone (organic lean)								Overburden Rock
Kolmule Fm.		Shale (organic lean, silty)								Overburden Rock
Kolje Fm.		Shale (typical)								Overburden Rock
Knurr Fm.		Shale (typical)								Overburden Rock
Hekkingen Fm.		Shale (organic rich, 8% TOC)	Value	10.00		Burnham(1989)_TII	Value	300.00		Source Rock
Fuglen Fm.		Shale (organic lean, siliceous, typical)								Seal Rock
Sto Fm.		Sandstone (typical)								Reservoir Rock
Nordmela Fm.		Siltstone (organic lean)								Overburden Rock
Tubaen Fm.		Sandstone (clay poor)								Reservoir Rock
Fruholmen Fm.		Siltstone (organic rich, 2-3% TOC)								Overburden Rock
Snadd Fm.		Siltstone (organic rich, 2-3% TOC)	Value	2.00		Burnham(1989)_TII	Value	150.00		Source Rock
Kobbe Fm.		Siltstone (organic rich, 2-3% TOC)	Value	3.00		Burnham(1989)_TIII	Value	200.00		Source Rock
Orret Fm.		Siltstone (organic lean)								Underburden Rock
Basement		BASEMENT								Underburden Rock



Table 5.6 Facies definition table for model 106

Name	Color	Lithology Value	TOC Mode	TOC Value [%]	TOC Map	Kinetics	HI Mode	HI Value [mgHC/gTOC]	HI Map	Petroleum System Elements
Nordland Gp		Siltstone (organic lean)								Overburden Rock
Torsk Fm		Shale (organic lean, typical)								Overburden Rock
Kveite-Kviting Fm		Siltstone (organic lean)								Overburden Rock
Kolmule Fm		Shale (organic lean, silty)								Overburden Rock
Kolje Fm		Shale (typical)								Overburden Rock
Knurr Fm		Shale (typical)								Overburden Rock
Hekkingen Fm		Shale (organic rich, 8% TOC)	Value	12.00		Burnham(1989)_TIII	Value	350.00		Source Rock
Fuglen Fm		Shale (organic lean, siliceous, t...								Seal Rock
Sto Fm		Sandstone (typical)								Reservoir Rock
Nordmela Fm		Siltstone (organic lean)								Overburden Rock
Tubaen Fm		Sandstone (typical)								Reservoir Rock
Fruholmen Fm		Siltstone (organic rich, 2-3% T...								Overburden Rock
Snadd Fm		Siltstone (organic rich, 2-3% T...	Value	3.00		Burnham(1989)_TIII	Value	250.00		Source Rock
Kobbe Fm		Siltstone (organic rich, 2-3% T...	Value	4.00		Burnham(1989)_TIII	Value	200.00		Source Rock
Orret Fm		Siltstone (organic lean)								Underburden Rock

## 5.6. Boundary Conditions

Boundary conditions define the basic energetic conditions for temperature and burial history of the source rock and, consequently, for the maturation of organic matter through time (Ben Awuah et al. 2013 and PetroBuilder 2D\_User Guide version 2014.1). Three main boundary conditions were defined during modelling of the basin these are; Paleo Water Depth (PWD), Sediment Water Interface Temperature (SWIT) and Heat Flow (HF). The PWD of the Hammerfest Basin was assigned based on Lambeck (1995) which varies between 300 and 500 m. The SWIT was defined using the automatic function in Petromod. The hemisphere was defined as northern and the latitude as 72° (Fig. 5.4). The hemisphere and latitude were set based on the location of the Hammerfest Basin. First the HF trend was created and then assigned to the model from 0 Ma (40 mW/m<sup>2</sup>) to 345 Ma (70 mW/m<sup>2</sup>). Heat flow values in the Barents Sea vary between 50-70 mW/m<sup>2</sup> (Eldhom et al., 1999). The highest value of 75 mW/m<sup>2</sup> has been assigned to periods of extensive rifting and faulting whereas the lowest heat flow values have been assigned to periods of uplift and erosion.

The boundary condition trends for both models are shown in Figs. 5.5 and 5.6 and Tables 5.7 and 5.8.

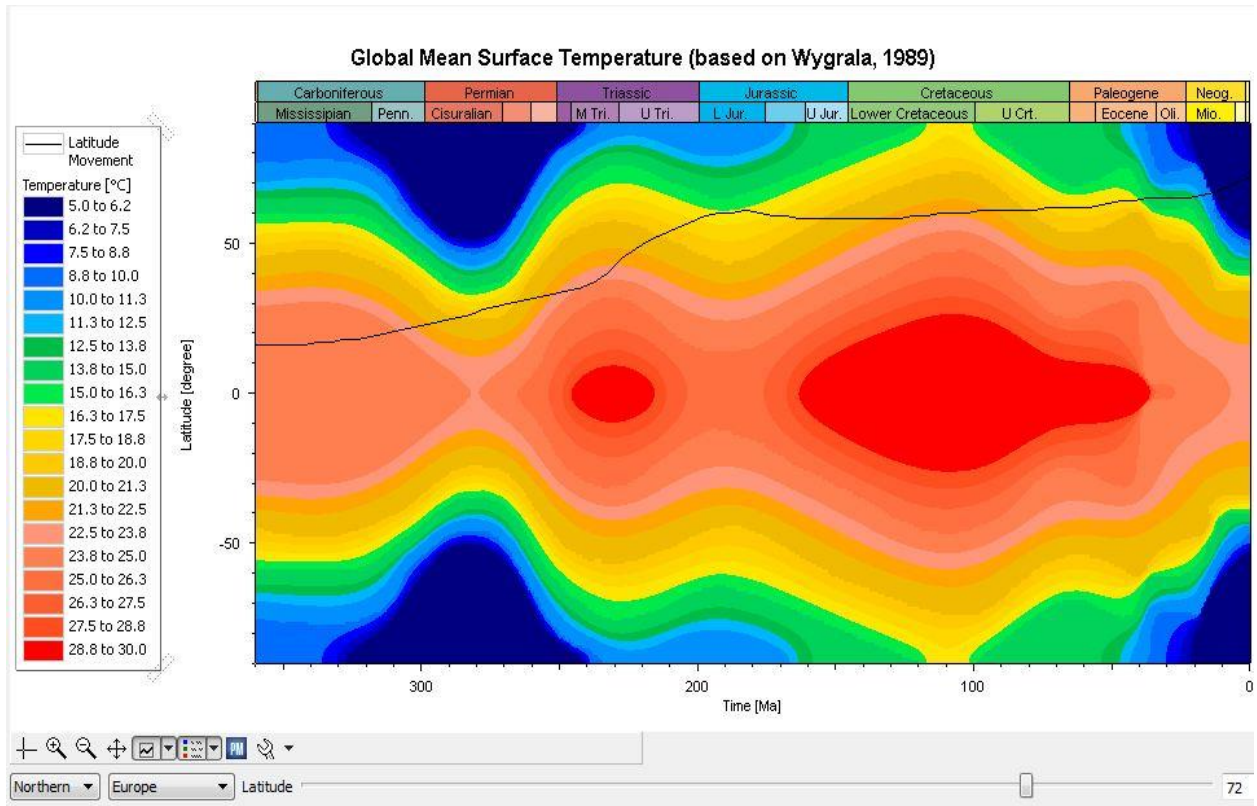


Figure 5.4 Sediment Water Interface Temperature (SWIT) definition.

Table 5.7 Boundary conditions for model 104

Age [Ma]	PWD [m]	Age [Ma]	SWT [°C]	Age [Ma]	HF mW/m <sup>2</sup>
0.00	300	0.00	2.75	117.50	63.49
5.65	304	5.65	2.78	118.80	63.96
8.48	325	8.48	2.94	120.00	64.45
11.30	306	11.30	2.79	121.30	64.95
14.13	300	14.13	6.50	122.50	65.46
16.96	306	16.96	6.47	123.80	65.99
19.78	305	19.78	8.38	125.00	66.53
22.61	307	22.61	9.68	126.30	67.09
25.43	300	25.43	10.27	127.50	67.65
28.26	304	28.26	10.27	128.80	68.23
31.09	302	31.09	10.50	130.00	68.82
33.01	320	33.01	10.70	131.30	69.41
36.74	301	36.74	11.47	132.50	70.00
39.57	301	39.57	12.06	133.80	70.59
42.39	302	42.39	13.13	135.00	71.17
45.22	303	45.22	13.92	136.30	71.72
48.04	312	48.04	14.10	137.50	72.23
50.87	321	50.87	14.16	138.80	72.68
53.70	330	53.70	14.38	140.00	73.04
56.52	325	56.52	14.38	141.30	73.28
59.35	309	59.35	14.61	142.50	73.36
62.17	304	62.17	14.63	143.80	73.27
65.00	305	65.00	14.70	145.00	73.02
67.83	302	67.83	14.85	147.60	72.33
69.30	305	69.30	14.96	150.10	71.54
72.52	309	72.52	15.24	152.60	70.66
75.06	312	75.06	15.51	155.20	69.67
78.65	315	78.65	16.15	157.80	68.57
81.95	320	81.95	16.39	160.30	67.34
85.00	308	85.00	16.45	162.90	66.00
90.00	301	90.00	17.11	165.40	64.54
120.85	315	120.80	17.90	167.90	62.97
125.95	304	125.90	17.76	170.50	61.29
138.36	304	138.40	17.21	173.10	59.53
150.45	301	150.40	16.40	175.60	57.72
158.56	301	158.60	15.81	178.10	55.89
164.74	307	164.70	14.62	180.70	54.09
170.85	306	170.90	13.60	183.30	52.37
173.86	312	173.90	13.15	185.80	50.79
176.46	319	176.50	12.92	188.40	49.44
182.00	301	182.00	12.63	190.90	48.37
190.40	307	190.40	12.56	193.40	47.68
196.00	308	196.00	12.65	196.00	47.39



Table 5.8 Boundary conditions for model 106

Age [Ma]	PWD [m]	Age [Ma]	SWIT [°C]	Age [Ma]	HF mW/m <sup>2</sup>
0.00	302	0.00	16.57	117.50	63.49
5.65	320	5.65	15.96	118.80	63.96
8.48	305	8.48	16.66	120.00	64.45
11.30	304	11.30	16.86	121.30	64.95
14.13	308	14.13	16.87	122.50	65.46
16.96	306	16.96	17.20	123.80	65.99
19.78	315	19.78	17.08	125.00	66.53
22.61	307	22.61	17.70	126.30	67.09
25.43	306	25.43	17.98	127.50	67.65
28.26	310	28.26	18.08	128.80	68.23
31.09	322	31.09	17.91	130.00	68.82
33.01	316	33.01	18.25	131.30	69.41
36.74	308	36.74	18.73	132.50	70.00
39.57	306	39.57	19.41	133.80	70.59
42.39	307	42.39	21.44	135.00	71.17
45.22	306	45.22	22.11	136.30	71.72
48.04	304	48.04	22.64	137.50	72.23
50.87	320	50.87	22.39	138.80	72.68
53.70	325	53.70	22.19	140.00	73.04
56.52	310	56.52	22.76	141.30	73.28
59.35	305	59.35	22.80	142.50	73.36
62.17	308	62.17	22.79	143.80	73.27
65.00	309	65.00	22.84	145.00	73.02
67.83	318	67.83	22.68	147.60	72.33
69.30	309	69.30	22.99	150.10	71.54
72.52	306	72.52	23.24	152.60	70.66
75.06	314	75.06	23.20	155.20	69.67
78.65	307	78.65	23.58	157.80	68.57
81.95	322	81.95	23.32	160.30	67.34
85.00	305	85.00	23.84	162.90	66.00
90.00	306	90.00	23.82	165.40	64.54
120.85	304	120.80	23.88	167.90	62.97
125.95	307	125.90	23.79	170.50	61.29
138.36	309	138.40	23.67	173.10	59.53
150.45	304	150.40	22.68	175.60	57.72
158.56	305	158.60	21.65	178.10	55.89
164.74	306	164.70	20.71	180.70	54.09
170.85	321	170.90	19.10	183.30	52.37
173.86	314	173.90	19.18	185.80	50.79
176.46	318	176.50	18.89	188.40	49.44
182.00	306	182.00	19.08	190.90	48.37
190.40	307	190.40	18.84	193.40	47.68
196.00	303	196.00	18.96	196.00	47.39

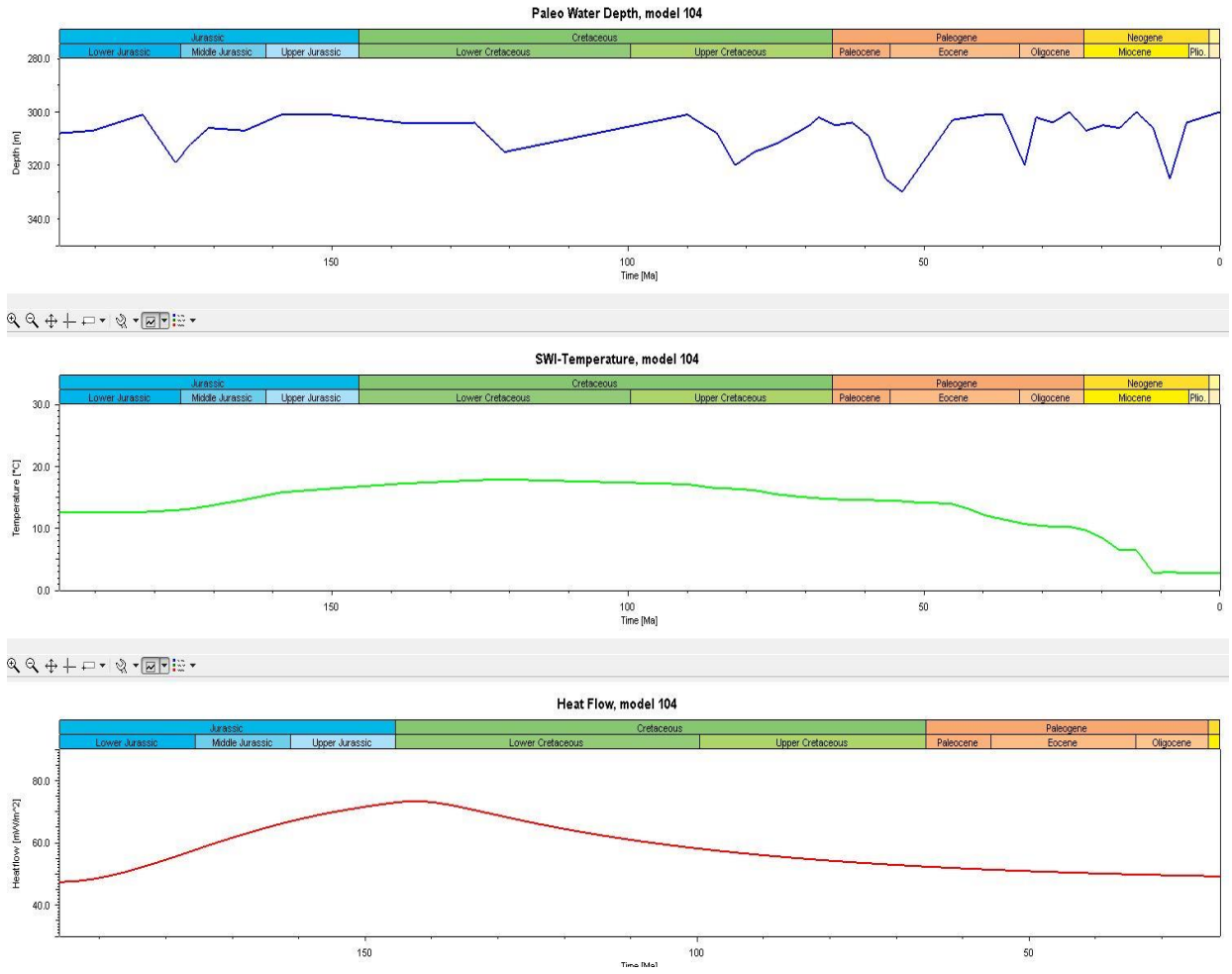


Figure 5.5 Boundary conditions trends for model 104.

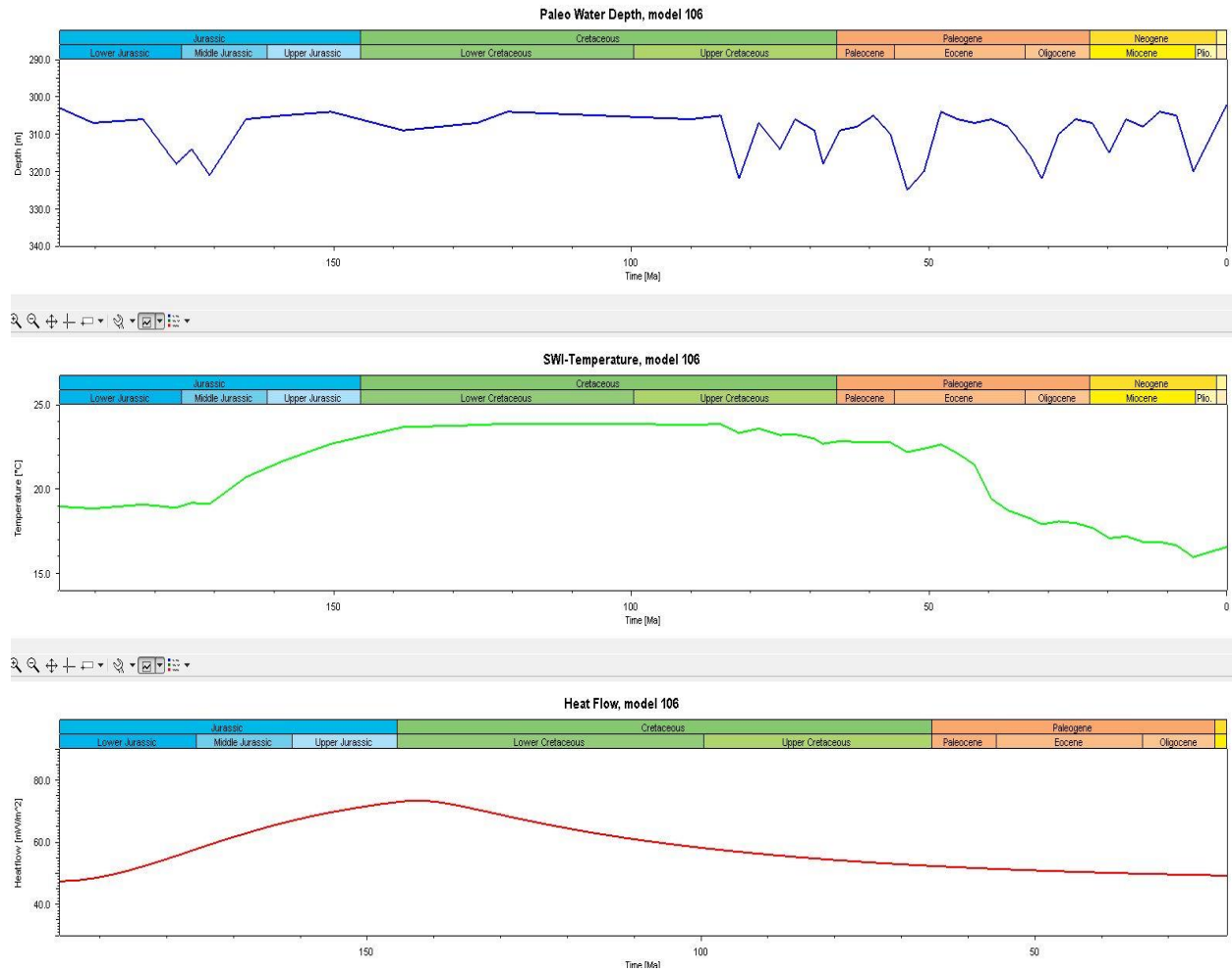


Figure 5.6 Boundary conditions trends for model 106.

## 5.7. Model Simulation

The model was opened in 2D simulator window to run for simulation. The migration method was hybrid (Darcy + Flow path) as explained by Ben Awuah et al., (2013). The default value was used for the parameters in the simulation option and run the control panes. Sweeney and Burnham (1990) `_EASY%Ro` and the kinetic reaction used was Burnham (1989) `_TII` and Burnham (1989) `_TIII` were used as for calibration model. The simulation run was successful and the log summary for both models is shown in Appendix 1 and 2.

## Chapter 6

### 6.0 MODELLING RESULTS AND DISCUSSION

#### 6.1 Burial History, Erosion and Uplift

The study area has been affected by several episodes of erosion and uplift during the Cenozoic which have affected the petroleum system. When the area is uplifted and then eroded it tends to be exposed to lower temperatures which can have a large effect on the maturity of the source rocks.

The Hammerfest Basin petroleum system plays consists of the source rocks of Triassic (Snadd and Kobbe Formations) and of Upper Jurassic (Hekkingen Formation) age. Reservoir rocks (Sto and Tubaen Formations) are of Middle to Upper Jurassic age, whereas the seal rocks (Fuglen and Hekkingen Formations) are Middle to Upper Jurassic. Both structural and stratigraphic traps are found in the basin. The maturation of the hydrocarbons from the Triassic and Upper Jurassic source rocks lead to the generation of large quantities of gas and oil in the area.

The area of study has been affected by several episodes of tectonic events since the Caledonian Orogeny in Early Devonian times. Mid Carboniferous rifting was followed during the Triassic to Early Jurassic by regional subsidence and large thicknesses of sediments were deposited from the eastern areas. During Middle to Late Jurassic rifting took place which lead to the formation of the current Hammerfest Basin. Figs. 6.1- 6.17 show the deposition of the layers in the basin.

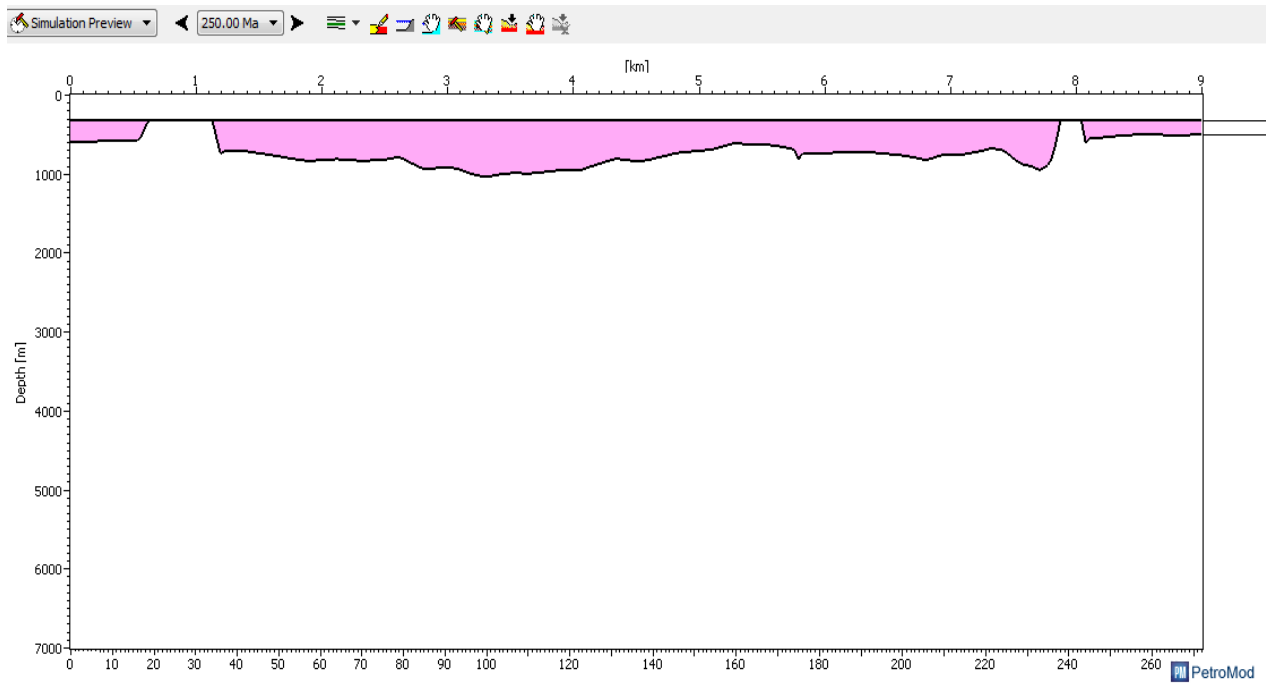


Figure 6.1 250-230 Ma, Orret Formation deposited at Early Triassic layer.

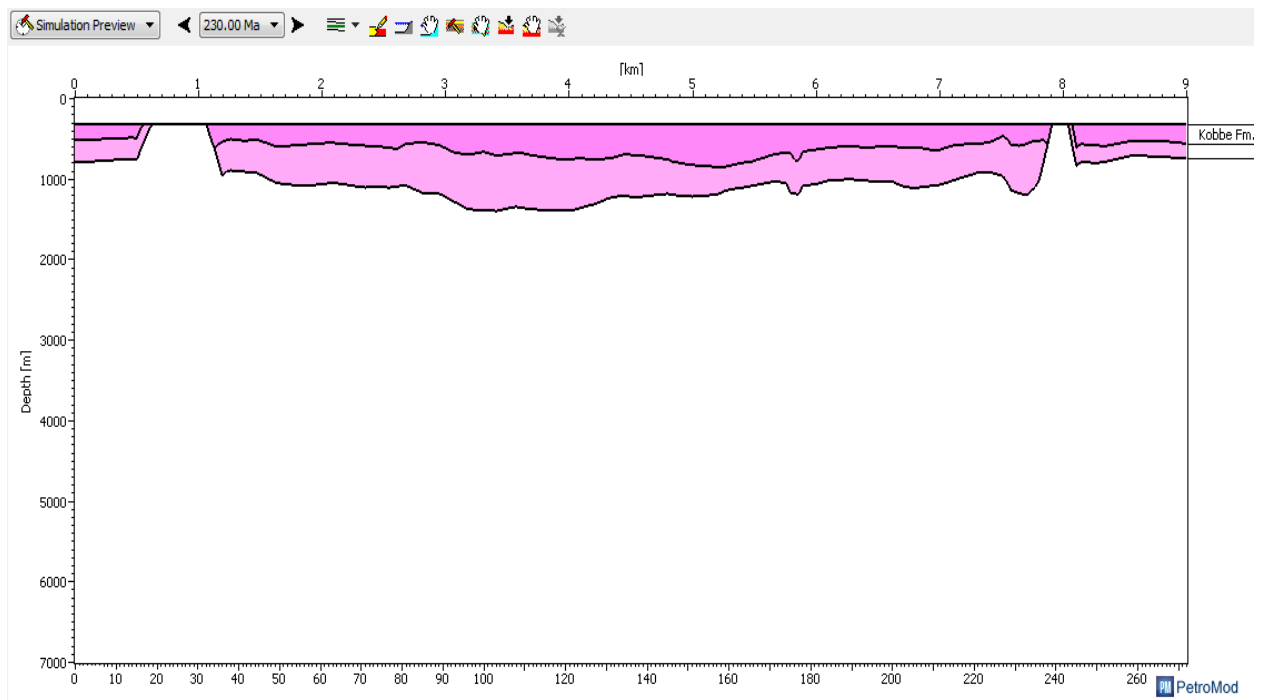


Figure 6.2 230-210 Ma, Kobbe Formation deposited at Middle Triassic layer.



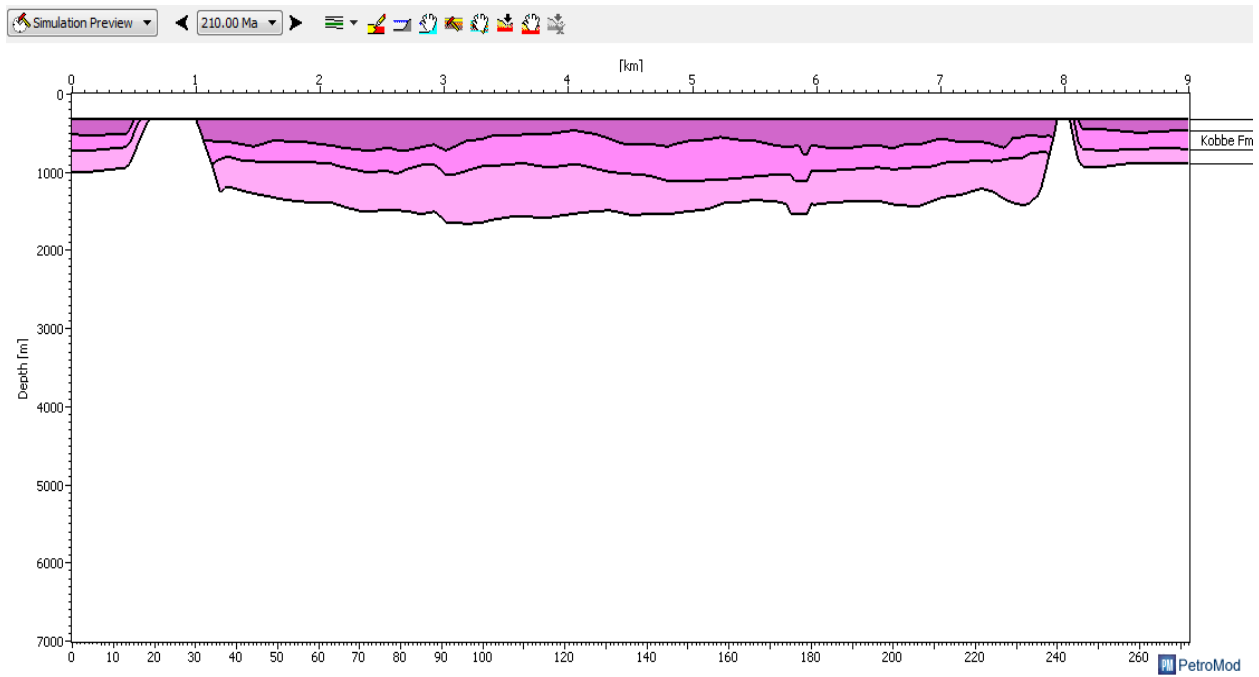


Figure 6.3 210 - 200 Ma, Snadd Formation deposited at Middle to Upper Triassic layer.

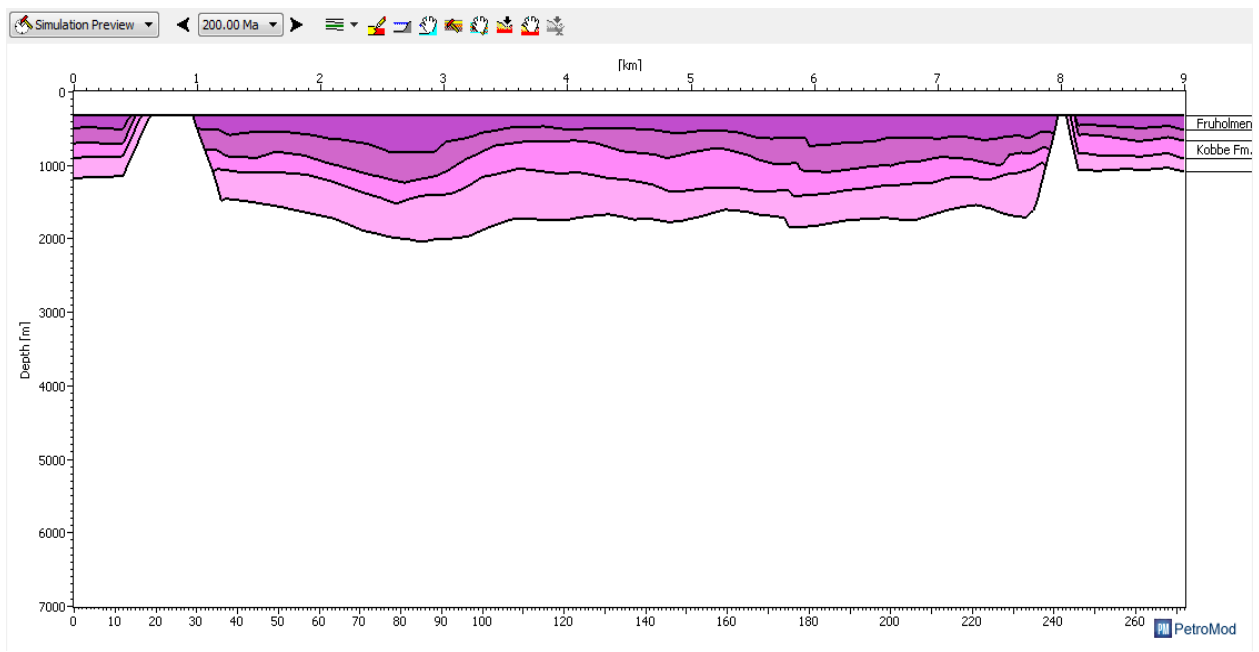


Figure 6.4 200 - 196 Ma, Fruholmen Formation deposited at Upper Triassic layer.

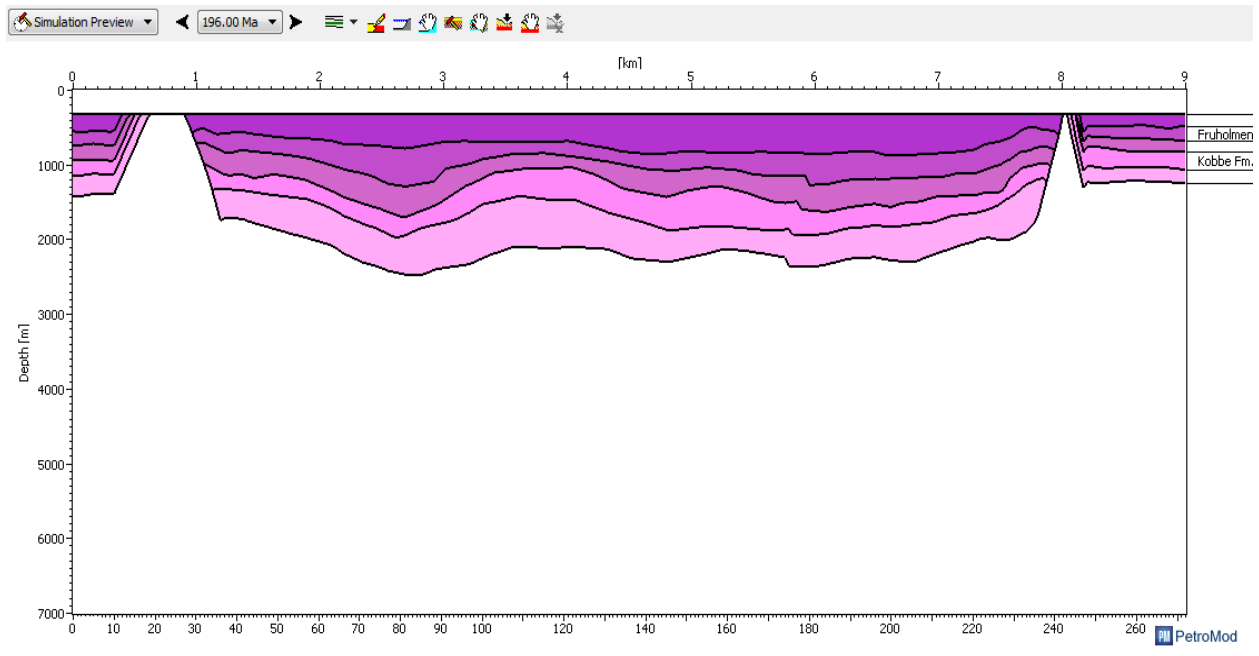


Figure 6.5 196 - 184Ma, Tubaen Formation deposited at Lower Jurassic layer.

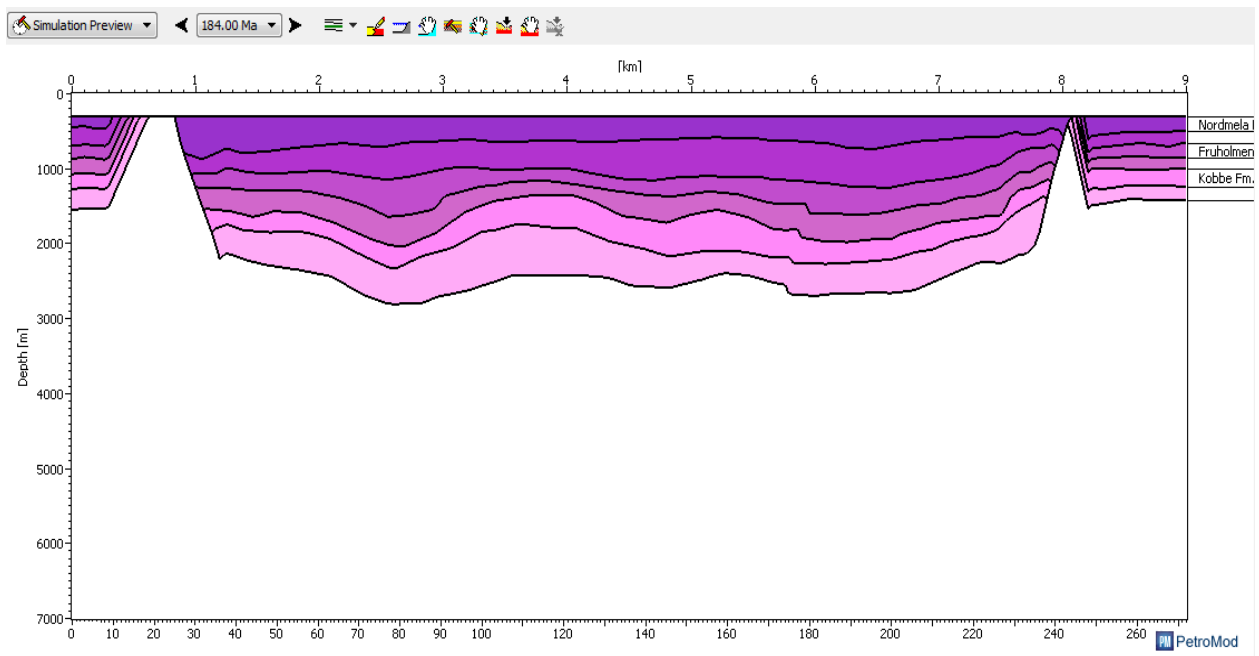


Figure 6.6 184 - 167 Ma, Nordmela Formation deposited at Lower to Middle Jurassic layer.

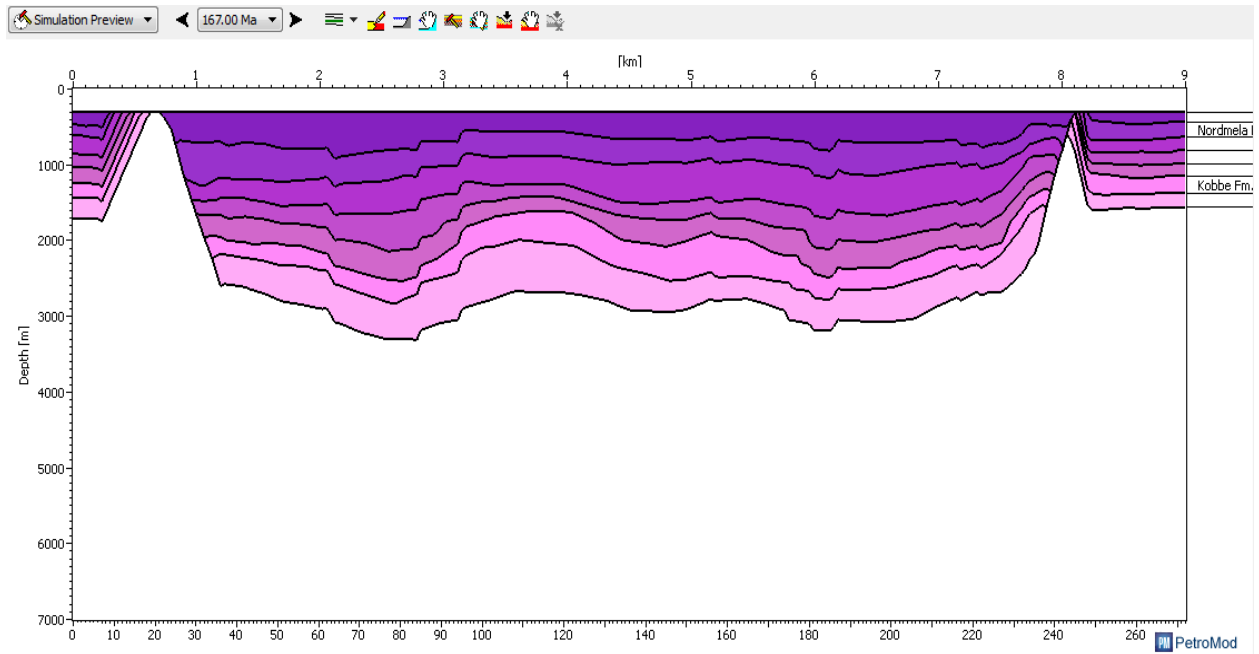


Figure 6.7 167- 155 Ma, Sto Formation deposited at Middle Jurassic layer.

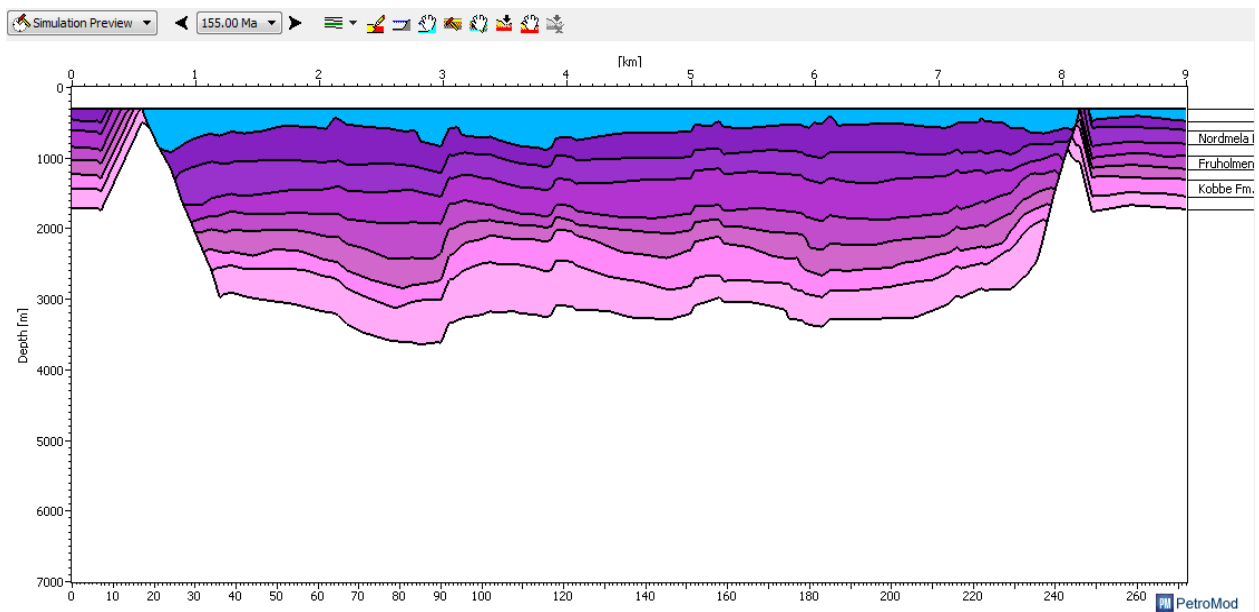


Figure 6.8 155 – 140 Ma, Fuglen Formation deposited at Middle to Upper Jurassic layer.

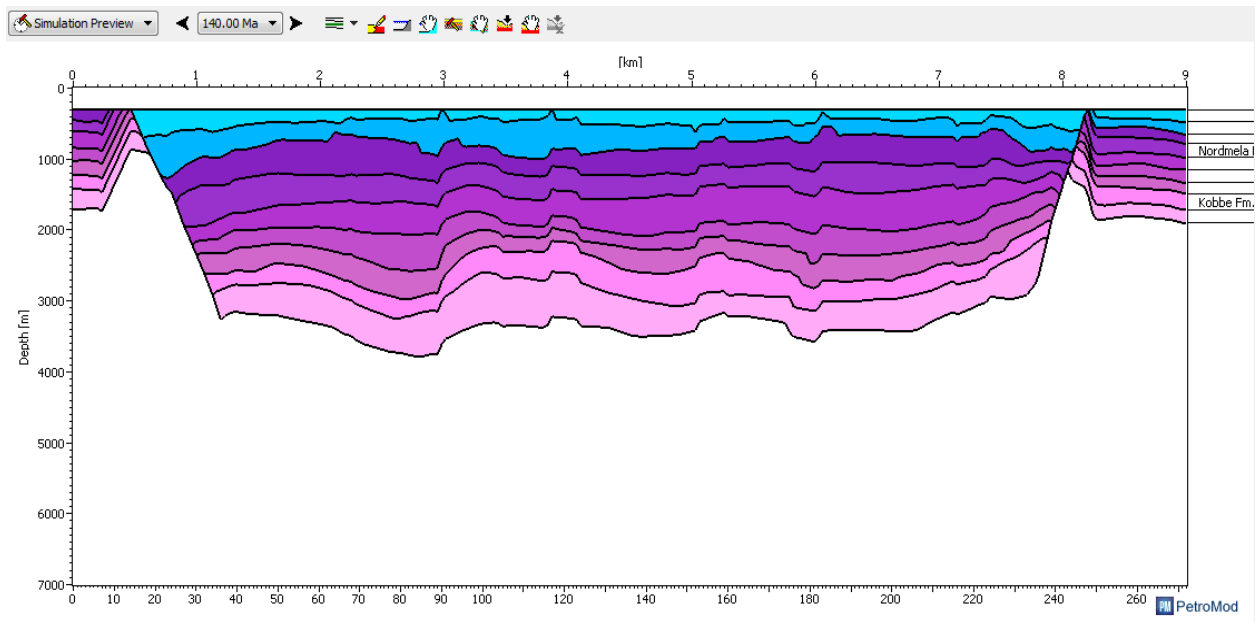


Figure 6.9 140 – 130 Ma, Hekkingen Formation deposited at Upper Jurassic to Lower Cretaceous layer.

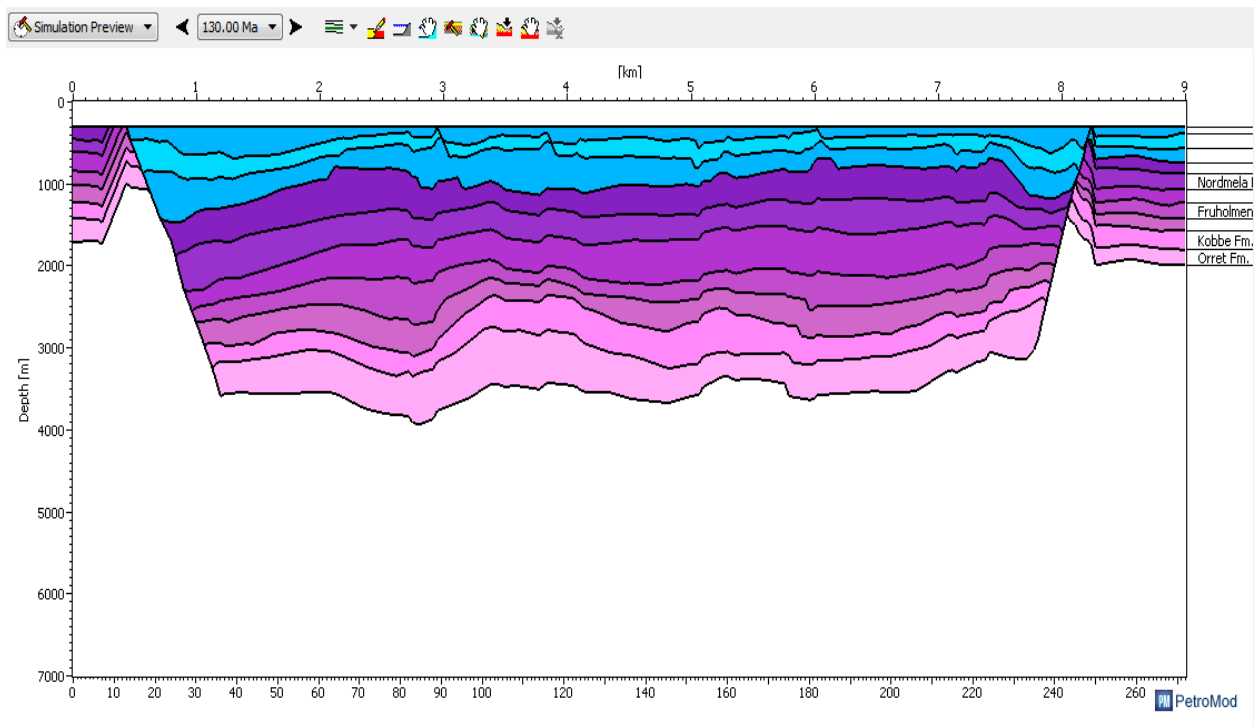


Figure 6.10 130 – 120 Ma, Knurr Formation deposited at Lower Cretaceous 1 layer.

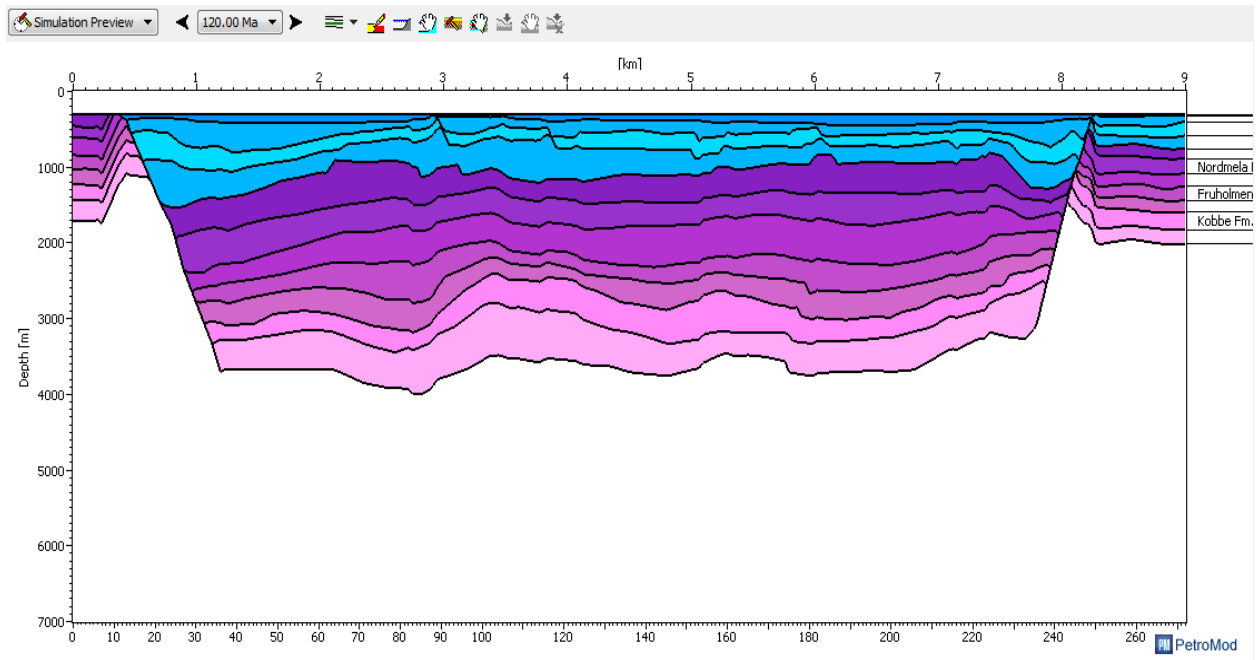


Figure 6.11 120 – 96 Ma, Kolje Formation deposited at Lower Cretaceous 2 layer.

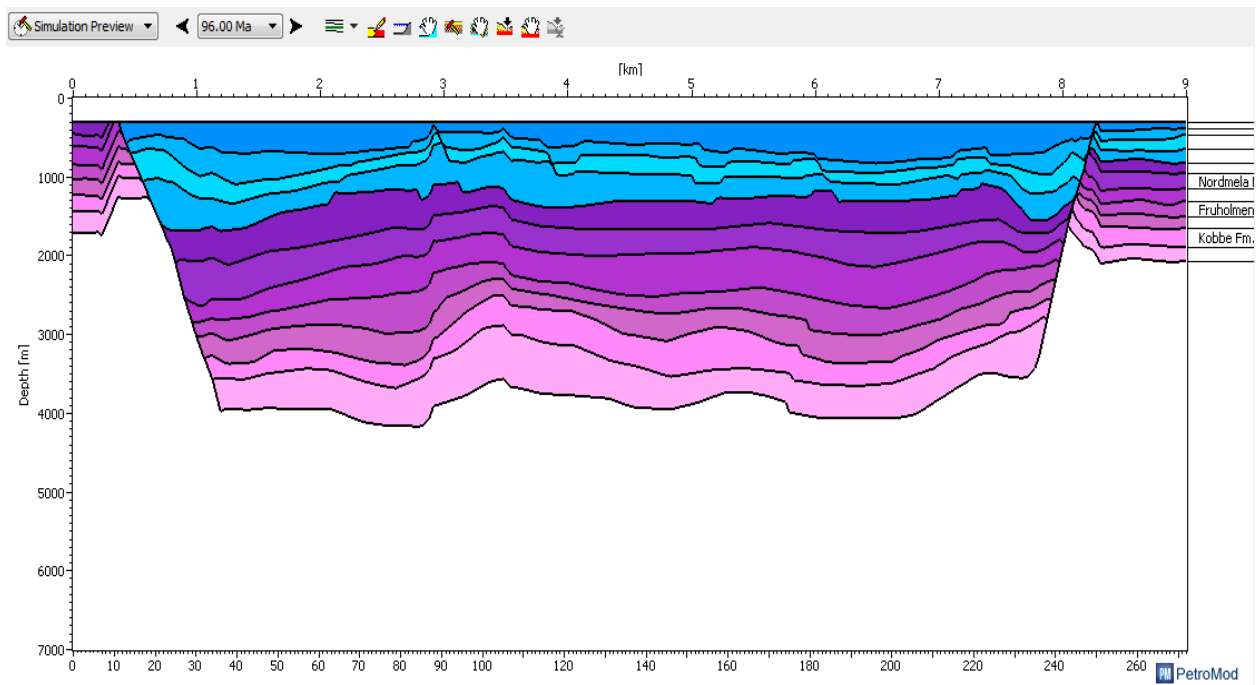


Figure 6.12 96 – 75 Ma, Kolmule Formation deposited at Lower Cretaceous 3 layer.

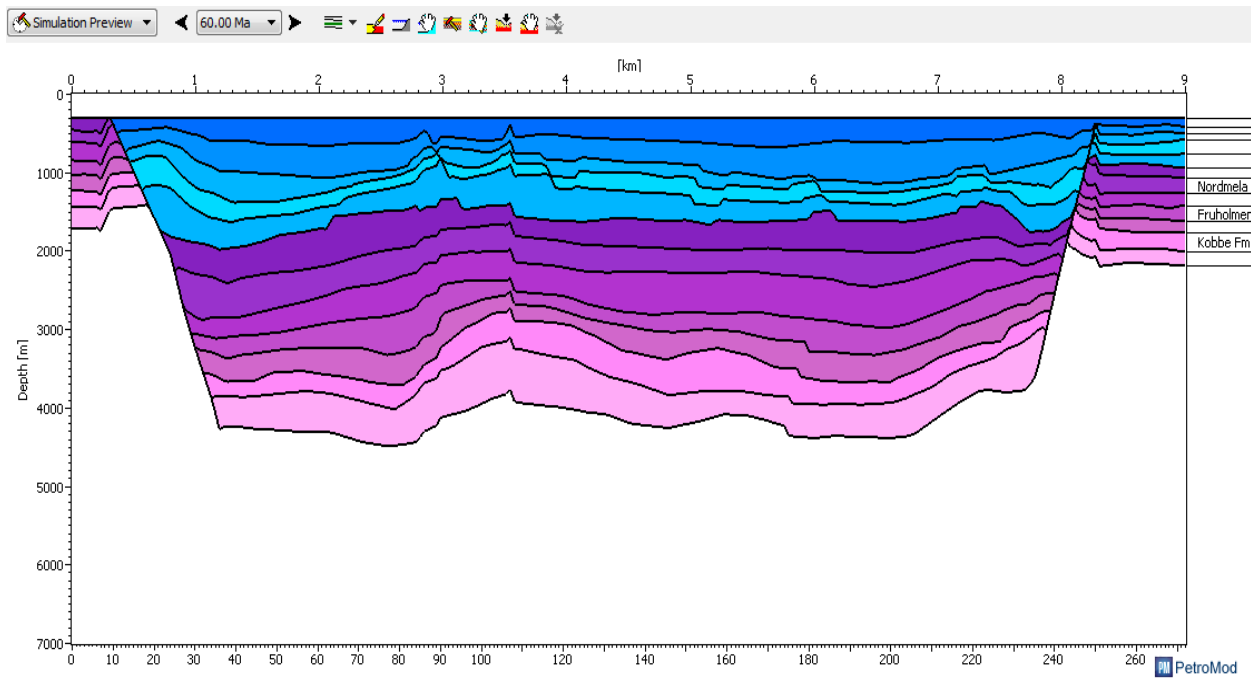


Figure 6.13 75 - 60 Ma, first erosion (uplift) of Kveite-Kviting Formation at Late Cretaceous layer, resulting in reduction of layer thickness of 200 m at Late Cretaceous.

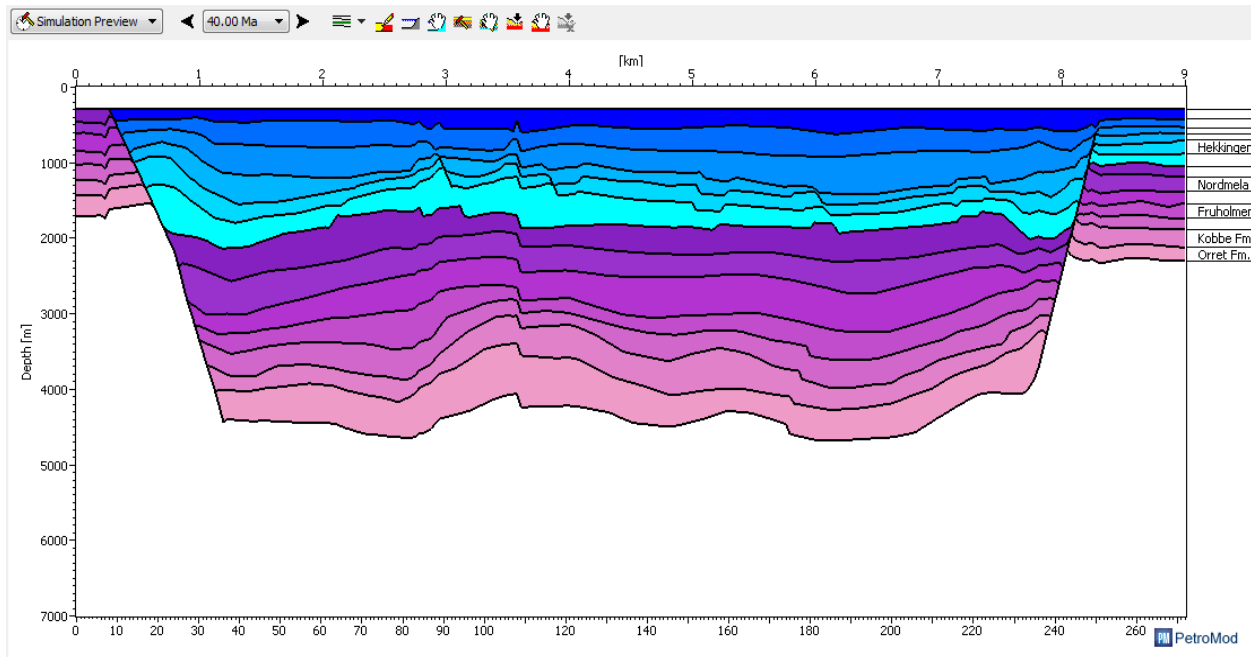


Figure 6.14 40-35 Ma, second erosion (uplift) of Base Paleocene layer, resulting in the reduction of layer thickness of 300 m at Paleocene.

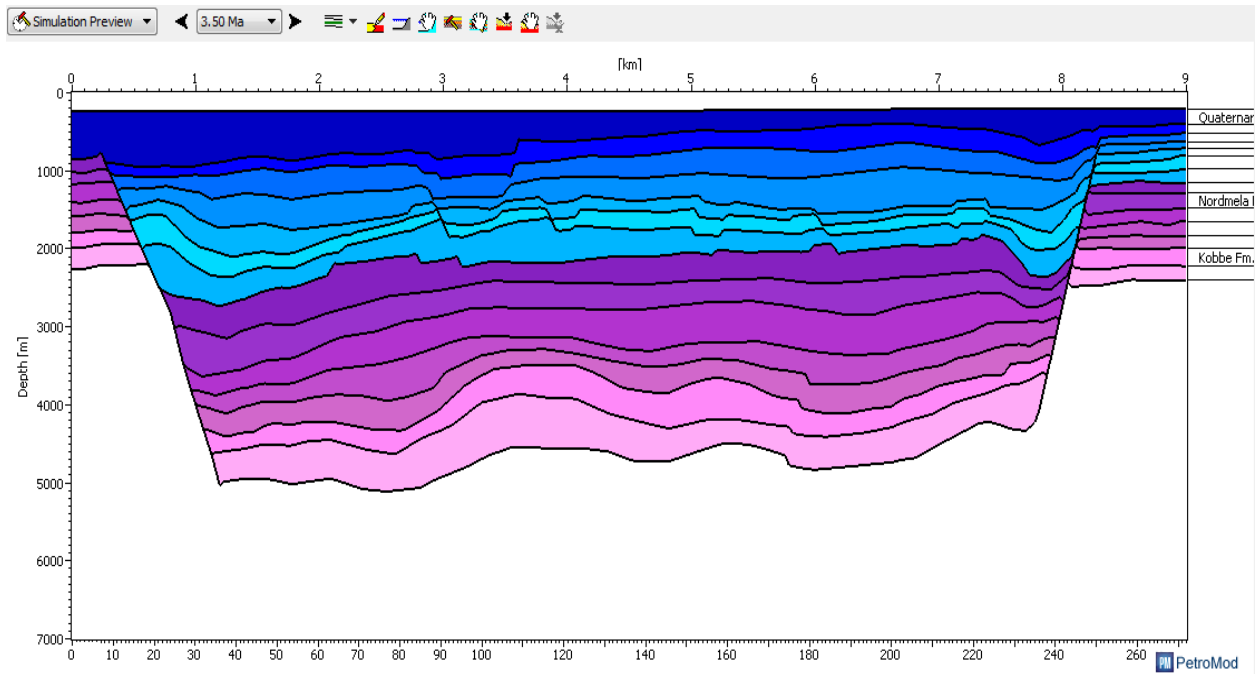


Figure 6.15 3.5 – 0.01 Ma, third erosion (uplift) of Base Quaternary layer, resulting in the reduction of layer thickness of 500 m at Paleogene.

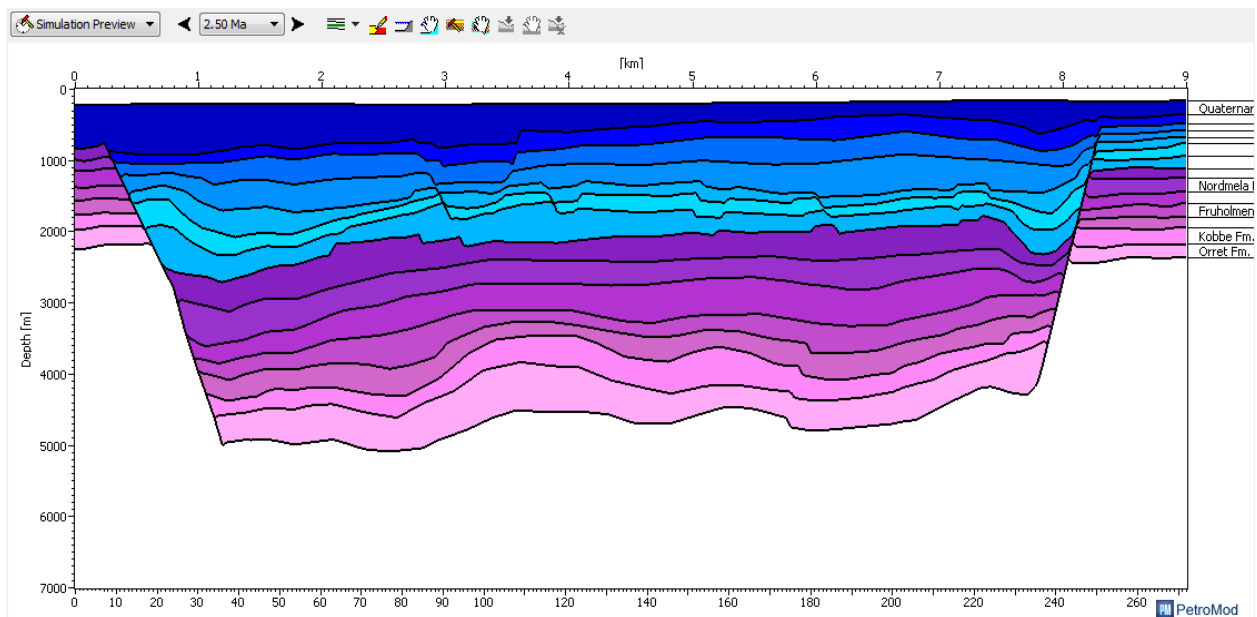


Figure 6.16 2.5 – 0.01 Ma, Deposition of the Quaternary layer.

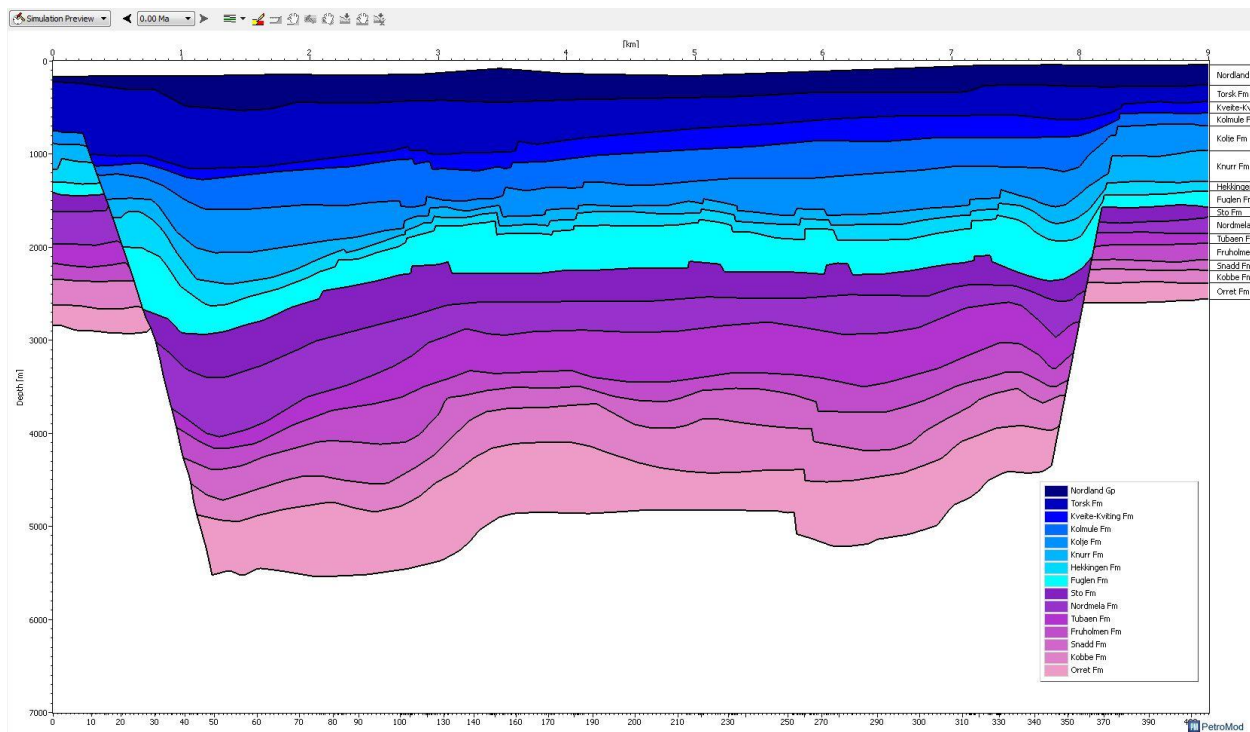


Figure 6.17 0.00 Ma, Present day basin configuration.

## 6.2. Source Rock Maturity

The modelling results of the Hammerfest Basin are viewed in PetroMod by using the 2D viewer option. The results show that the Triassic source rocks are mature enough to produce hydrocarbons with the help of maturity parameters such as temperature and vitrinite reflectance which was used in the calibration. The temperature history of the model shows that the base of the sediments in the deeper parts of the basin reaches maximum temperatures of about 250 °C in model 104 and 245 °C in model 106. The source rocks of the Snadd and Kobbe Formations reached maximum temperature at about 220 °C in model 104 (Fig 6.18) and 225 °C in model 106 (Fig 6.19). The source rock Hekkingen Formation reaches maximum temperature at about 85 °C in model 104 and 75 °C in model 106. These ranges of temperature provides evidence that the Triassic source rocks (Snadd and Kobbe Formations) are over matured and reaches the dry gas window in the deepest parts of the basin whereas the Hekkingen Formation is still in matured stage to generate oil. The uplift and erosion which took place trigger the cooling of the source rocks, this lead to the cessation in hydrocarbon generation as evidenced by Hekkingen Formation source rock in the model.



Both temperature and vitrinite reflectance increases with depth, thus they show linear relationship between temperature and vitrinite reflectance. The source rocks are matured enough to generate both oil and gas as shown by Vitrinite reflectance by (Sweeney & Burnham (1990)), which is the standard indicator for maturity.

The maturation of the Triassic source rocks started during Mid-Cretaceous when early oil generated, this shown by temperature and vitrinite reflectance from the model. The deeper sediments of the Hammerfest Basin experience higher temperature around 220 °C, which resulted to high vitrinite reflectance value. Thus, the deeper part of the basin was transformed earlier to produce hydrocarbons and high maturity occurs at this area compared to the rest of the basin. However, the less deep sediments such as of Mid-Cretaceous its sediment temperature was around 75-85 °C, whereas the vitrinite reflectance value was in the range of 0.55-0.7 which indicate the oil mature stage (Figs. 6.20 and 6.21).

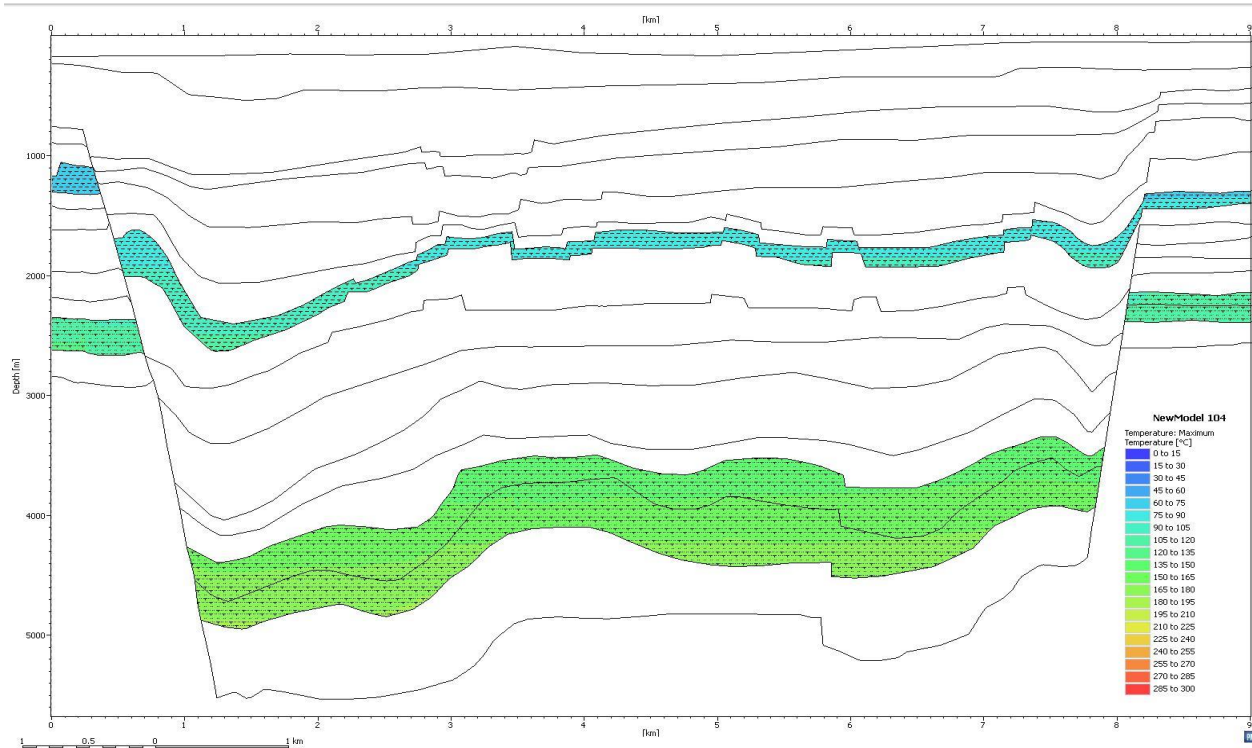


Figure 6.18 Present day temperature of the source rocks intervals for model 104.

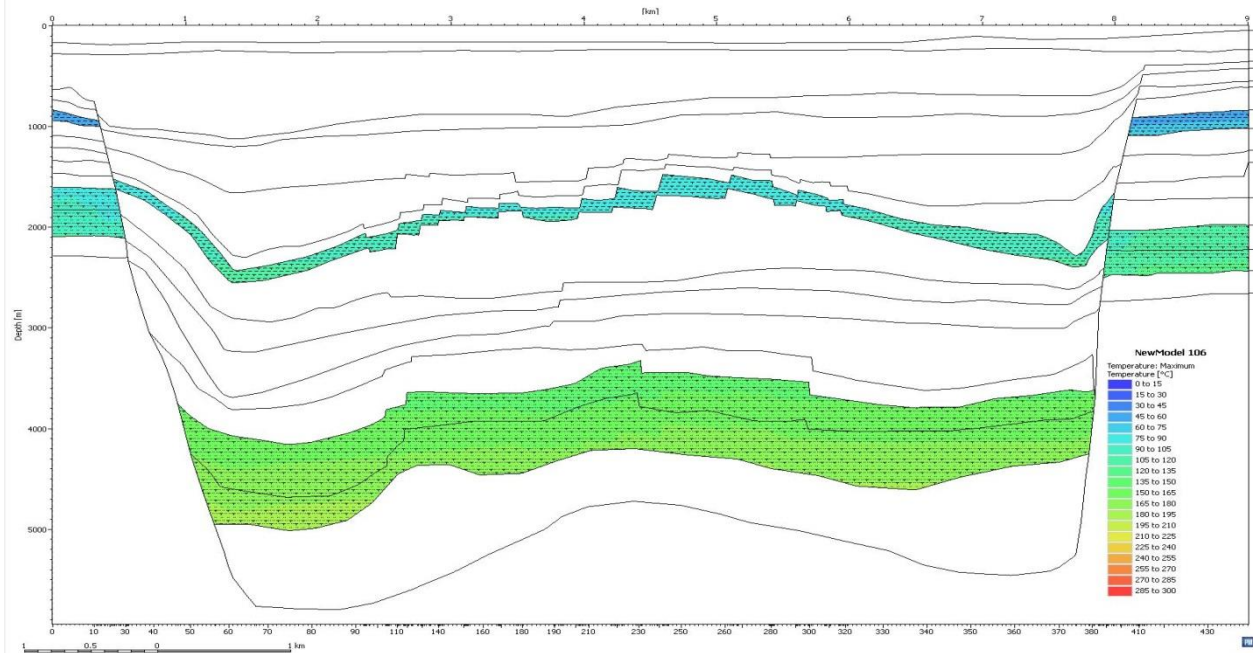


Figure 6.19 Present day temperature of the source rocks intervals for model 106.

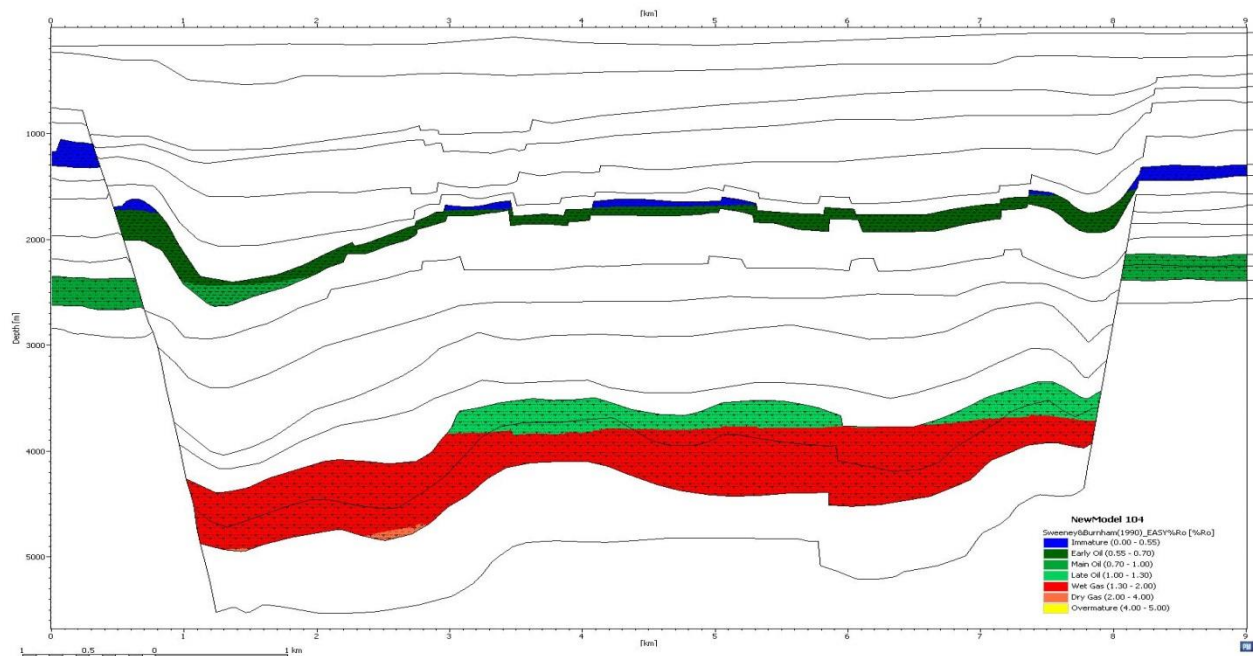


Figure 6.20 Present day Easy Ro converted in oil and gas generation windows for model 104.

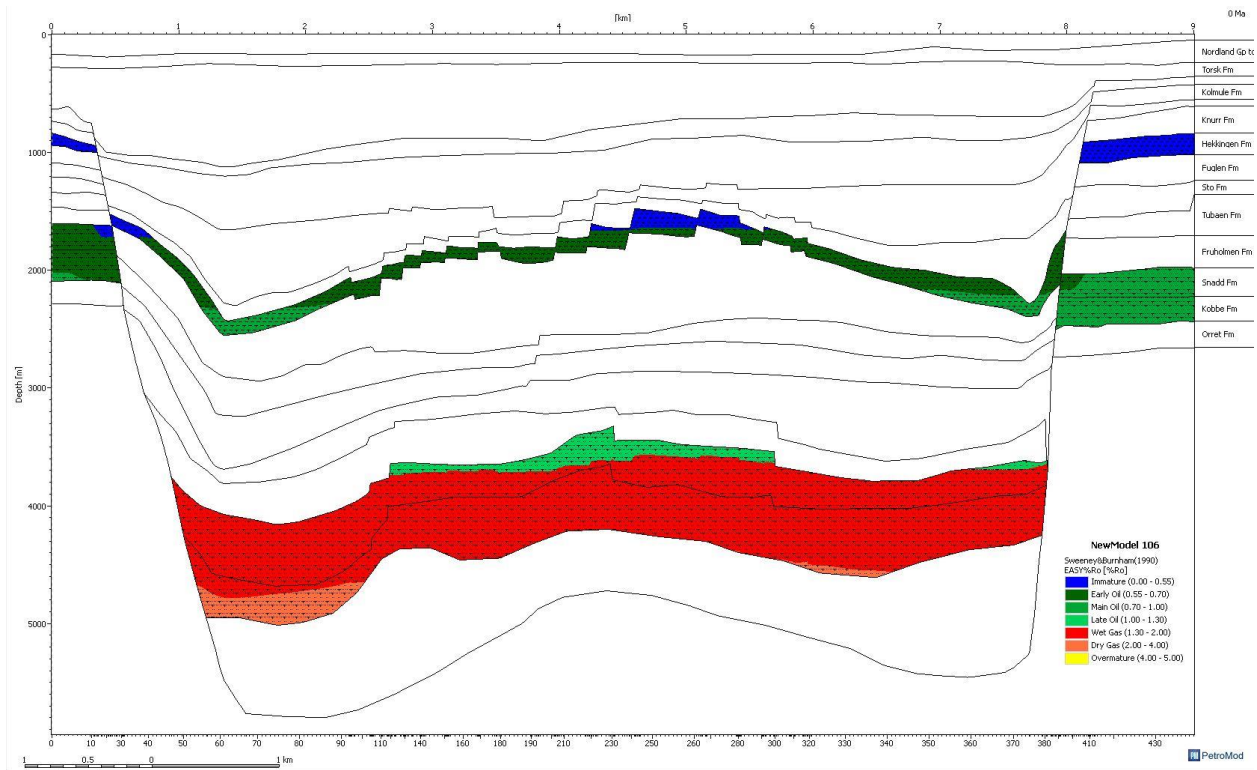


Figure 6.21 Present day Easy Ro converted in oil and gas generation windows for model 106.

Transformation ratio (TR) is the maturity indicator which shows that the source rock is matured enough to transform kerogen to oil or gas. When the value of TR of the source rock reaches 1, it is fully matured and all hydrocarbons have been generated from the source rocks. For immature source rocks the TR value is 0. The Hammerfest Basin models 104 and 106 indicate in deeper part of the basin, the transformation of the source is 1 and other parts 0.42 – 0.70 is already transformed. So, the model result show that Late Jurassic (Hekkingen Formation) is immature at present day and the Middle to Late Triassic (Snadd and Kobbe Formations) are nearly fully mature (Figs. 6.22 and 6.23). More increase in temperature can triggers the generation of the remaining kerogen bulk in the Hammerfest Basin (Figs. 6.24 and 6.25).

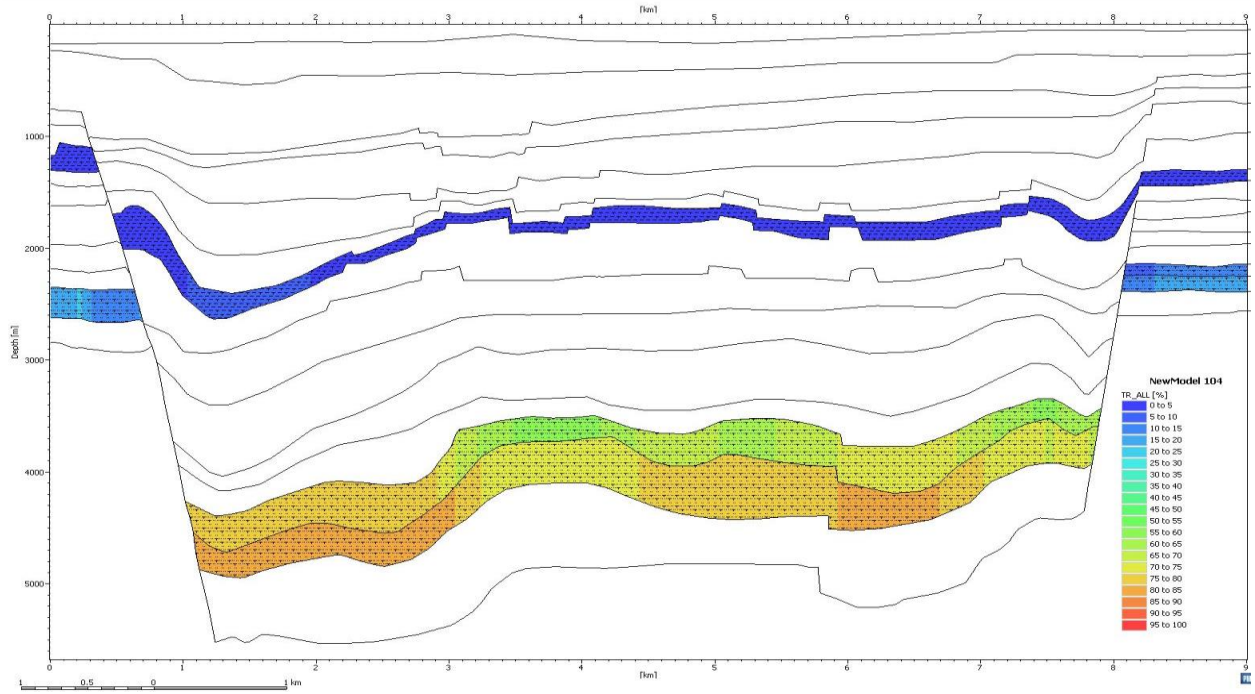


Figure 6.22 Present day transformation ratio for model 104.

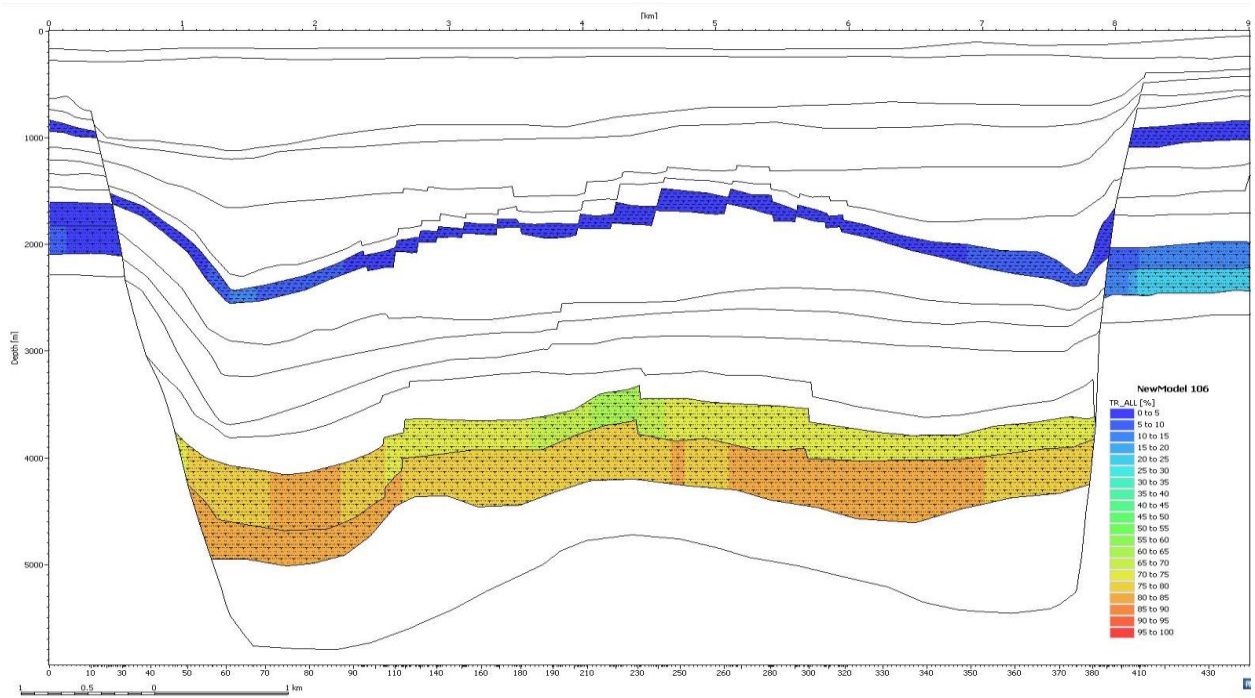


Figure 6.23 Present day transformation ratio for model 106.



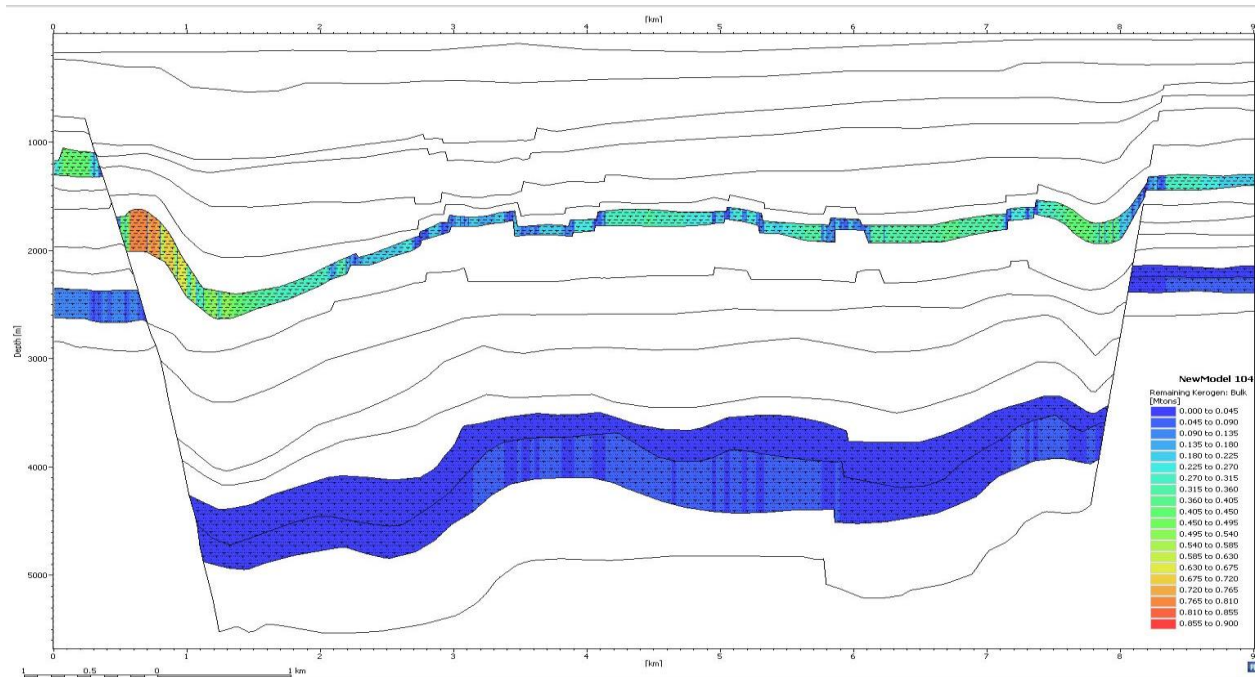


Figure 6.24 Present day remaining kerogen bulk for model 104.

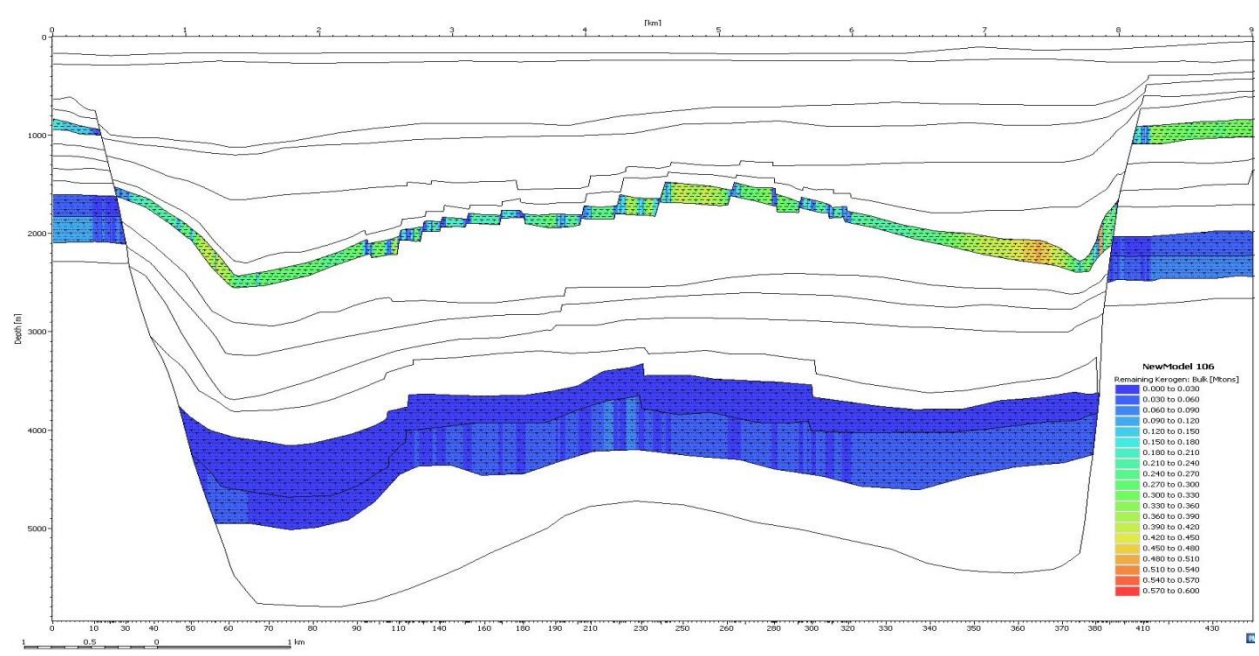


Figure 6.25 Present day remaining kerogen bulk for model 106.

### 6.3. Hydrocarbon Generation, Migration and Accumulation

The petroleum system was formed by the combination of petroleum system elements, processes and timing during deposition of the layers. The deposition of the petroleum elements such as reservoir, source and seal rocks should occur before petroleum system processes such as generation, migration and accumulation took place. During Mid Cretaceous time generation, migration and accumulation of hydrocarbons had started to occur, the preservation of hydrocarbons depends on the formation of the traps. The results of the model show that traps formed during Late Jurassic to Early Cretaceous which means that the preservation of the hydrocarbons generated was possible due to the proper timing of the trap formation. The Sto and Tubaen reservoir was formed during Early to Middle Jurassic before the generation of the hydrocarbons from the source rocks. Since these events occurred at the proper timing, then it was possible for the hydrocarbons to migrate and accumulate in the reservoirs. A critical moment is the point in time selected by the investigator that best depicts the generation, migration and accumulation of the hydrocarbons in a petroleum system (Magoon and Dow 1994). The critical moment which is represented by red line in Fig. 6.26, is considered to be 80 Ma.

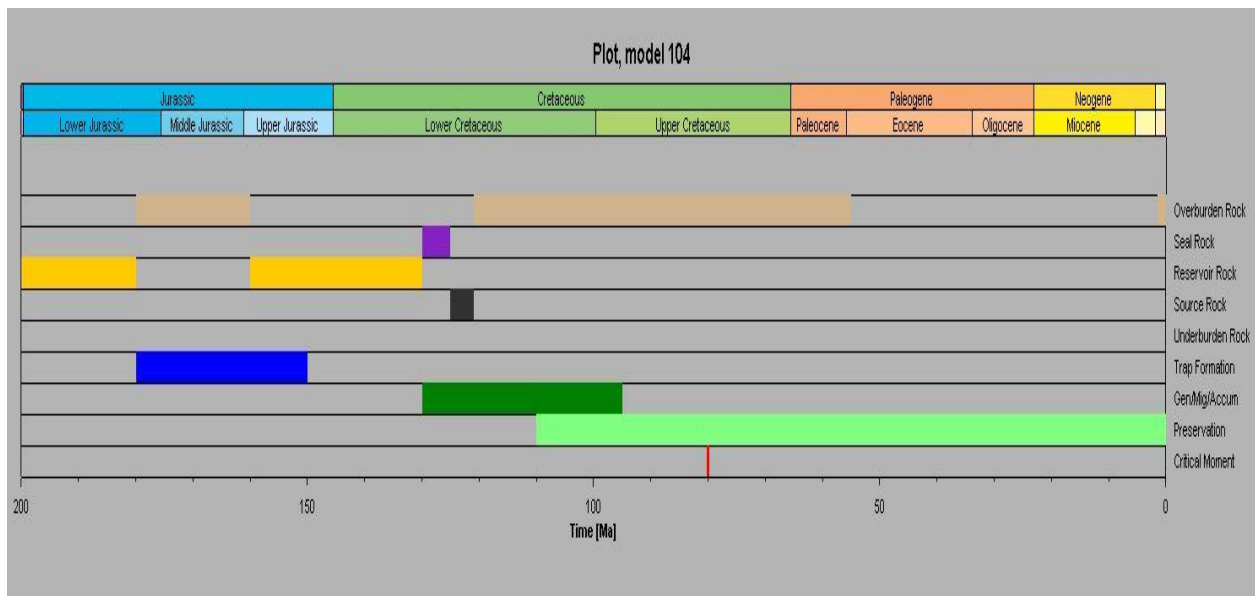


Figure 6.26 Event chart.

The accumulation of hydrocarbons is not possible to occur before the deposition of the petroleum system elements such as reservoir and seal being deposited. The migration of the hydrocarbons are vertically upward or downward from the source rock (where they are generated) into the reservoir rock. The possibility of the reservoir which is near to source rocks to receive hydrocarbons is higher compared to those which are far from the source. In the model our reservoirs are in between the younger and older source rocks, thus we expect the migration to be vertically upward and downward. Some migration occurs along faults which cause leakage of hydrocarbons (Figs. 6.27 and 6.28) and accumulated in the layers above.

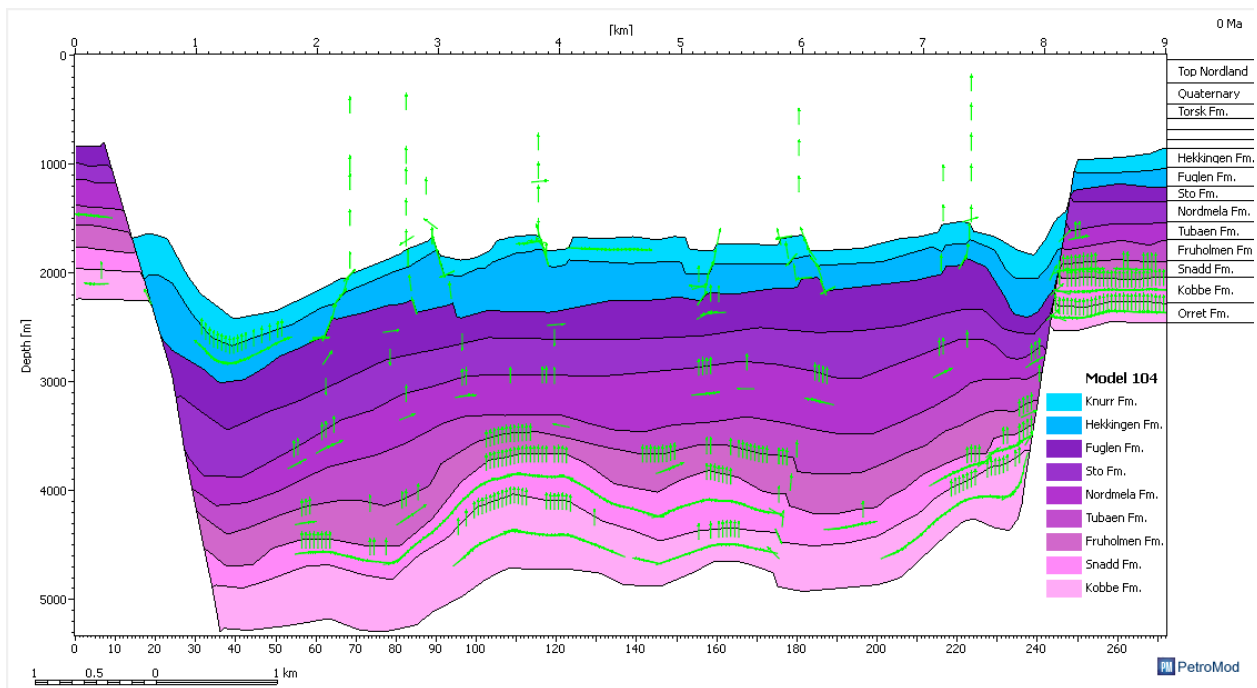


Figure 6.27 Oil upward migration from the source rocks into the reservoirs and the lateral migration within the source rocks.

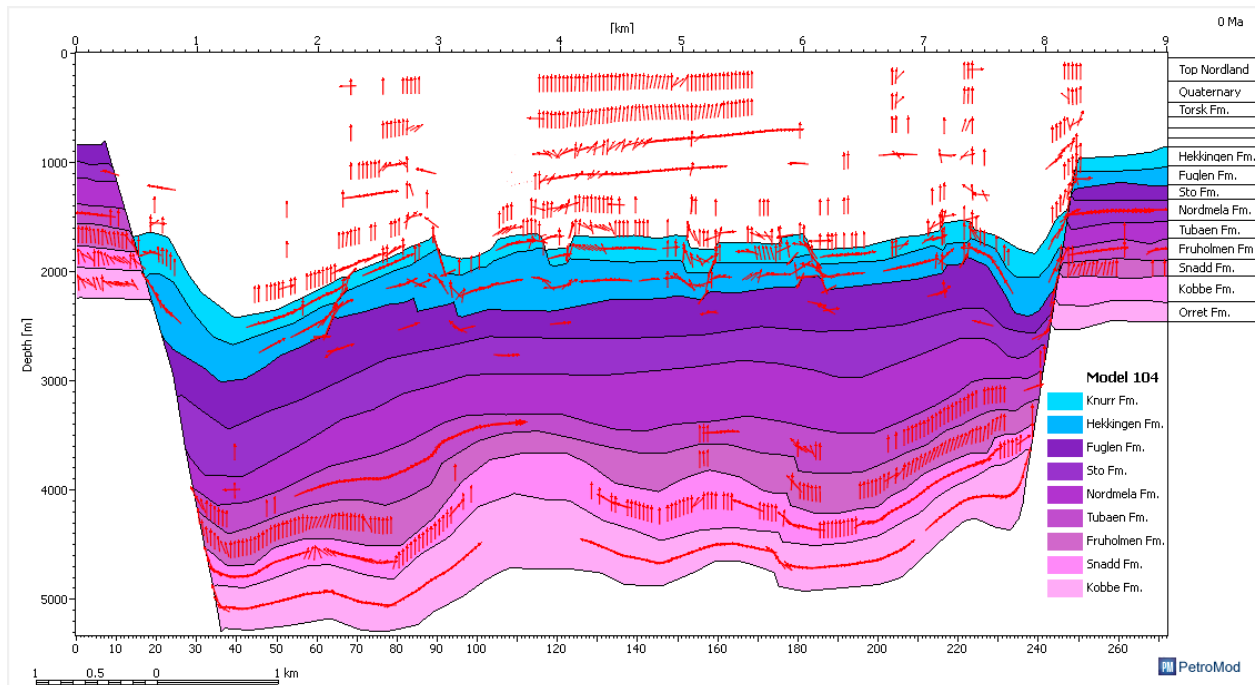


Figure 6.28 Gas upward migration from the source rocks into the reservoirs and the lateral migration within the source rocks.

The model results show that there are possible prospects and accumulated hydrocarbon reserves present in the study area. The visible accumulation at reservoir conditions is about 29.65 MMbbls of oil and 8.06 Mm<sup>3</sup> of gas, whereas the amount flashed to surface condition are 21.44 MMbbls of oil and 2567.33 Mm<sup>3</sup> of gas (Model 104). Model 106 show the visible accumulation at reservoir conditions is about 34.19 MMbbls of oil and 11.11 Mm<sup>3</sup> of gas, whereas 24.69 MMbbls and 3017.82 Mm<sup>3</sup> of gas are flashed to the surface conditions



## Chapter 7

### 7.0 CONCLUSION

Tectonic events of Late Carboniferous to Early Cretaceous age in the western part of the Barents Sea lead to the evolution of the Hammerfest Basin through extension of the faulted blocks. The formation of the major faults zones (Astrias Fault Complex (AFC) and Troms-Finnmark Fault Complex (TFFC)) which separate the Hammerfest Basin from the Loppa High to the north and the Troms-Finnmark Platform to the south was a major tectonic event in the evolution of the Hammerfest Basin, which culminated in Late Jurassic to Early Cretaceous rifting event.

The petroleum system of the Hammerfest Basin was formed during Triassic to Paleocene. The petroleum plays of the Hammerfest Basin consist of the geological factors such as source rocks, the Snadd and Kobbe Formations of Triassic age and the Hekkingen Formation of the Upper Jurassic age. The reservoir rocks (Sto and Tubaen Formations) are of Middle to Lower Jurassic age. The seal/cap rocks consist of the Fuglen and, Hekkingen Formations of Middle to Upper Jurassic age and Early Cretaceous shales. The traps formed largely as structural traps such as rotated fault block traps and some stratigraphic traps like pinch outs.

The potential Triassic source rocks of the area are highly matured and have generated large quantities of the hydrocarbons. The maturity of the source rocks has been modelled by using vitrinite reflectance (EasyRo) and transformation ratio. The Hekkingen Formation of Late Jurassic age is also considered as the potential source rock, but it is not well enough matured. The modelling shows that in the deeper parts (Triassic) of the basin the source rocks have become matured to overmatured, but in the shallower parts (Late Jurassic) hydrocarbons continue to be generated to the present day. The basin is heavily faulted. A lot of the vertical migration will have taken place along faults

The late Cenozoic uplift and erosion in the Hammerfest Basin has affected the seal causing the leakage of hydrocarbons in some parts of the basin. The temperature decrease due to uplift and erosion caused cooling of the source rocks that lead to the cessation in hydrocarbon generation.

## REFERENCES

- Ben-Awuah, J., WemazenuAdda, G., and Mijinyawa, A. (2013). 2D Basin Modelling and Petroleum System Analysis of the Triassic Play in the Hammerfest Basin of the Norwegian Barents Sea. *Research Journal of Applied Sciences, Engineering and Technology*, 6(17):3137–5150.
- Berglund, L., Augustson, J., Faerseth, R., Gjelberg, J., and Ramberg-Moe, H. (1986). The evolution of the Hammerfest Basin. In: *Habitat of hydrocarbons on the Norwegian Continental Shelf*. 319–338.
- Breivik, A. J., Faleide, J. I. & Gudlaugsson, S. T. (1998). Southwestern Barents Sea margin: late Mesozoic sedimentary basins and crustal extension. *Tectonophysics*, 293, 21–44.
- Bugge, T., Mangerud, G. et al. (1995). The Upper Paleozoic succession on the Finnmark Platform, Barents Sea. *Norwegian Journal of Geology*, 75, 3–30.
- Cavanagh, A. J., Di Primio, R., Scheck-Wenderoth, M., and Horsfield, B. (2006). Severity and timing of Cenozoic exhumation in the southwestern Barents Sea. *Journal of the Geological Society*, 163(5):761–774.
- Dalland, A., Worsley, D. & Ofstad, K. (eds) (1988). *A Lithostratigraphical Scheme for the Mesozoic and Cenozoic Succession Offshore Mid- and Northern Norway*. Norwegian Petroleum Directorate, Bulletins, 4, 1–65
- Dallmann, W. K. (1999). *Lithostratigraphic lexicon of Svalbard: review and recommendations for nomenclature use: Upper Palaeozoic to Quaternary bedrock*. . Committee on the Stratigraphy of Svalbard/NorskPolarinstitutt. 320 pp.
- Dore, A.G. and L.N. Jensen, (1996). The impact of late Cenozoic uplift and erosion on hydrocarbon exploration: Offshore Norway and some other uplifted basins. *Glob. Planet. Change*, 12(1-4): 415-436.
- Dore, A.G. and Lundin, E. R. (1996). Cenozoic compressional structures on the NE Atlantic margin: nature, origin and potential significance for hydrocarbon exploration. *Petroleum Geoscience*, 2, 299–311.

- Dore, A. G., Lundin, E. R., Birkeland, Ø., Eliassen, P. E. & Jensen, L.N. (1997). The NE Atlantic margin: implications of late Mesozoic and Cenozoic events for hydrocarbon prospectivity. *Petroleum Geoscience*, 3, 117–131.
- Eidvin, T., Jansen, E. & Riis, F. (1993). Chronology of tertiary fan deposits off the western Barents Sea; implications for the uplift and erosion history of the Barents Sea. *Marine Geology*, 112, 109–131.
- Eldhom, O., E. Sundvor, P.R. Vogt, B.O. Hjelstuen, K. Crane, A.K. Nilsen and T.P. Gladchenko, (1999). SW Barents Sea continental margin heat flow and Hakon Mosby mud volcanoes. *Geo-Mar. Lett.*, 19(1): 29-37.
- Etris, E. L., Crabtree, N. J., Dewar, J. & Pickford, S. (2001). True depth conversion: More than a pretty picture. *CSEG recorder*, 26, 11-22.
- Faleide, J. I., Vagnes, E. & Gudlaugsson, S. T. (1993). Late Mesozoic–Cenozoic evolution of the southwestern Barents Sea in a regional rift-shear tectonic setting. *Marine and Petroleum Geology*, 10, 186–214.
- Faleide, J. I., Solheim, A., Fiedler, A., Hjelmestuen, B. O., Andersen, E. S. & Vanneste, K. (1996). Late Cenozoic evolution of the western Barent Sea–Svalbard continental margin. *Global Planetary Change*, 12, 53–74.
- Gabrielsen, R. H., Faereth, R. B., and Jensen, L. N. (1990). Structural Elements of the Norwegian Continental Shelf. Pt. 1. The Barents Sea Region. Norwegian Petroleum Directorate. NPD Bulletin No 6.
- Gabrielsen, R., Gunnaleite, I. & Ottesen, S. (1993). Reactivation of fault complexes in the Loppa High area, southwestern Barents Sea. In: Vorren, T. O., Bergsager, E. et al. (eds) *Arctic Geology and Petroleum Potential*. Elsevier, Amsterdam/Norwegian Petroleum Society, Trondheim, Special Publications, 2, 631–641.
- Gabrielsen, R.H. (1984). Long lived fault zones and their influence on the tectonic development of the south-western Barents Sea. *J.Geol.Soc.*, London, 141, 651-662.

- Galloway, W. (1989). Genetic stratigraphic sequences in basin analysis I: Architecture and genesis of flooding surface bounded depositional units. *American Association of Petroleum Geologists Bulletin*, 73, 125–142.
- Gee, D. G., Fossen, H., Henriksen, N. & Higgins, A. K. (2008). From the early Paleozoic platforms of Baltica and Laurentia to the Caledonide orogen of Scandinavia and Greenland. *Episodes*, 31, 44–51.
- Gjelberg, J. & Steel, R. J. (1995). Helvetiafjellet Formation (Barremian-Aptian), Spitsbergen: characteristics of a transgressive succession. In: Steel, R. J., Felt, V. L., Johannessen, E. P. and Mathieu, C. (eds) *Sequence Stratigraphy on the Northwest European Margin*. Elsevier, Amsterdam/Norwegian Petroleum Society, Trondheim, Special Publications, 5, 571–593.
- Hantschel, T. & Kauerauf, A. I. (2009). *Fundamentals of Basin and Petroleum Systems Modeling*, Springer Science & Business Media.
- Hendricks, B.W.H. (2003). Cooling and denudation of the Norwegian and Barents Sea Margins, Northern Scandinavia. PhD thesis, Vrije Universiteit Amsterdam.
- Hendriks, B.W.H. & Andriessen, P.A.M. (2002). Pattern and timing of the post- Caledonian denudation of northern Scandinavia constrained by apatite fission track thermochronology. In: Dore, A.G., Cartwright, J.A., Stoker, M.S., Turner, J.P. & White, N.J. (eds) *Exhumation of the North Atlantic Margin: Timing, Mechanisms and Implications for Petroleum Exploration*. Geological Society, London, Special Publications, 196, 117–137.
- Henriksen, E., Bjørnseth, H. M. et al. (2011). Uplift and erosion of the greater Barents Sea: impact on prospectivity and petroleum systems. In: Spencer, A. M., Embry, A. F., Gautier, D. L., Stoupakova, A. V. & Sørensen, K. (eds) *Arctic Petroleum Geology*. Geological Society, London, *Memoirs*, 35, 271–281.
- Lambeck, K. (1995). Constraints on the Late Weichselian icesheet over the Barents Sea from observations of raised shorelines. *Quaternary Science Reviews*, 14(1):1–16.
- Larssen, G. B., Elvebakk, G. et al. (2005). Upper Palaeozoic lithostratigraphy of the southern part of the Norwegian Barents Sea. *Norges Geologiske Undersøkelser Bulletin*, 444, 3–43.

Larssen, G., Elvebakk, G., Henriksen, L. B., Kristensen, S., Nilsson, I., Samuelsen, T., Svånå, T., Stemmerik, L., and Worsley, D. (2002). Upper Palaeozoic lithostratigraphy of the Southern Norwegian Barents Sea. *Norwegian Petroleum Directorate Bulletin*, 9:76.

Leith, T. L., Weiss, H. M. et al. (1993). Mesozoic hydrocarbon source-rocks of the Arctic region. In: Vorren, T. O., Bergsager, E. et al. (eds) *Arctic Geology and Petroleum Potential*. Elsevier, Amsterdam/Norwegian Petroleum Society, Trondheim, Special Publications, 2, 1–25

Lien, T., Midtbø, R. E. & Martinsen, O. J. (2006). Depositional facies and reservoir quality of deep marine sandstones in the Norwegian Sea. *Norwegian Journal of Geology*, 86, 71–92.

Magoon, L. B. & Dow, W. G. (1994). *The Petroleum System— From Source to Trap*: AAPG Memoir, 60, 3-24.

Mørk et al. 1999b Mørk, A., Dallmann, W. K. et al. (1999). Mesozoic Lithostratigraphy. In: Dallmann, W. K. (ed.) *Lithostratigraphic Lexicon of Svalbard: Upper Paleozoic to Quaternary Bedrock. Review and Recommendation for Nomenclature Use*. Norwegian Polar Institute, Tromsø, 127–214.

Mørk, A. and Elvebakk, G. (1999). Lithological description of subcropping lower and middle Triassic rocks from the Svalis Dome, Barents Sea. *Polar Research*, 18, 83–104.

Mørk, A., Elvebakk, G. et al. (1999). The type section of the Vikinghøgda formation: a new Lower Triassic unit in central and eastern Svalbard. *Polar Research*, 18, 51–82

Mørk, A., Knarud, R. and Worsley, D. (1982). Depositional and diagenetic environment of the Triassic and lower Jurassic succession of Svalbard. In: Embry, A. & Balkwill, H. R. (eds) *Arctic Geology and Geophysics*. Canadian Society of Petroleum Geologists, Alberta, Memoirs, 8, 371–298.

Nilsen, K. T., Henriksen, E. & Larssen, G. B. (1993). Exploration of the Late Palaeozoic carbonates in the southern Barents Sea – a seismic stratigraphic study. In: Vorren, T. O., Bergsager, E. et al. (eds) *Arctic Geology and Petroleum Potential*. Elsevier, Amsterdam/ Norwegian Petroleum Society, Trondheim, Special Publications, 2, 393–402.

Nilsen, K. T., Vendeville, B. C. & Johansen, J.-T. (1995). Influence of regional tectonics on halokinesis in the Nordkapp Basin, Barents Sea. In: Jackson, M. P. A., Roberts, D. G. and Snelson,

S. (eds) Salt Tectonics: a Global Perspective. American Association of Petroleum Geologists, Tulsa, OK, Memoirs, 65, 413–436.

Norwegian Petroleum Directorate (2004). The Norwegian Petroleum Directorate archive of geological plays for the southern Barents Sea. <http://www.npd.no/English/Emner/Ressursforvaltning/CoverPage.htm>

Nøttvedt, A., Berglund, L. T., Rasmussen, E. & Steel, R. (1988). Some aspects of Tertiary tectonics and sedimentation along the western Barents Shelf. In: Morton, A. C. & Parsons, L. M. (eds) Early Tertiary Volcanism and the opening of the North Atlantic. Geological Society, London, Special Publications, 39, 421–425.

Oduro, P. (1998). The sedimentary evolution of the southwestern Barents Sea. PhD thesis, University of Oslo.

Ohm, S. E., Karlsen, D. A., and Austin, T. (2008). Geochemically driven exploration models in uplifted areas: Examples from the Norwegian Barents Sea. AAPG Bulletin, 92(9):1191–1223.

Richardson, G., Vorren, T. O. & Tøruðbakken, B. O. (1993). Cretaceous uplift and erosion in the southern Barents Sea: a discussion based on analysis of seismic interval velocities. Norwegian Journal of Geology, 73, 3–20.

Ritzmann, O. & Faleide, J. I. (2009). The crust and mantle lithosphere in the Barents Sea/Kara Sea region. Tectonophysics, 470, 89–104.

Rodrigues Duran, E., di Primio, R., Anka, Z., Stoddart, D., and Horsfield, B. (2013). 3D-basin modelling of the Hammerfest Basin (southwestern Barents Sea): A quantitative assessment of petroleum generation, migration and leakage. Marine and Petroleum Geology, 45:281–303.

Rønnevik, H., Beskow, B., and Jacobsen, H. P. (2009). Structural and Stratigraphic evolution of the Barents Sea. Canadian Society of Petroleum Geologist, Memoir 8(1982).

Ryseth, A., Augustson, J.H. & Charnock, M. et al. (2003). Cenozoic stratigraphy and evolution of the Sørvestsnaget Basin, southwestern Barents Sea. Norsk Geologisk Tidsskrift, 83, 107–130.

Samuelsberg, T., Elvebakk, G. & Stemmerik, L. (2003). Late Palaeozoic evolution of the Finnmark Platform, southern Norwegian Barents Sea. Norwegian Journal of Geology, 83, 351–362

Smelror, M., Petrov, O. V., Larssen, G. B. & Werner, S. (eds) (2009). Atlas. Geological History of the Barents Sea. Geological Survey of Norway, Trondheim.

Steel, R. J., Gjelberg, J., Helland-Hansen, W., Kleinspehn, K. L., Nøttvedt, A. & Larsen, M. R. (1985). The Tertiary strike-slip basins and orogenic belt of Spitzbergen. In: Biddle, K. & Christie-Blick, N. (eds) Strike-slip Deformation, Basin Formation, and Sedimentation. Society of Economical Paleontologists and Mineralogists, Tulsa, OK, Special Publications, 37, 339–359.

Steel, R.J. and Worsley, D. (1984). Svalbards post Caledonian strata-an atlas of sedimentational patterns and palaeogeographic evolution. In: Spencer, A. M. et al. (eds.), Petroleum Geology of the North European Margin, Norwegian Petrol. Soc., Graham and Trotman, London. 109-135.

Stemmerik, L. (2000). Late Palaeozoic evolution of the North Atlantic margin of Pangea. Palaeogeography, Palaeoclimatology, Palaeoecology, 161, 95–126.

Stemmerik, L., Elvebakk, G. & Worsley, D. (1999). Upper Palaeozoic carbonates reservoirs on the Norwegian Arctic Shelf: delineation of reservoir models with application to the Loppa high. Petroleum Geoscience, 5, 173–187.

Stemmerik, L. & Worsley, D. (2005). 30 years on – Arctic Upper Palaeozoic stratigraphy, depositional evolution and hydrocarbon prospectivity. Norwegian Journal of Geology, 85, 151–168.

Stemmerik, L. (1997). Permian (Artinskian–Kazanian) cool-water carbonates in north Greenland, Svalbard and the western Barents Sea. In: James, N. P. & Clarke, J. A. D. (eds) Cool-water Carbonates. Society of Economical Paleontologists and Mineralogists, Tulsa, OK, Special Publications, 56, 349–364.

Sweeney, J.J. and A.K. Burnham, (1990). Evaluation of a simple model of vitrinite reflectance based on chemical kinetics. AAPG Bull., 74: 1559-1570.

Talleraas, E., (1979). The Hammerfest basin-an aulacogen? Proceedings of the Norwegian Sea Symposium. Norwegian Petroleum Society, NSS/18, pp: 1-13.

Telford, W. M., Sheriff, R. E. (1980). Reflection Interpretation. Applied Geophysics. pp 260-264

Vigran, J. O., Mangerud, G., Mørk, A., Bugge, T. & Weitschat, W. (1998). Biostratigraphy and sequence stratigraphy of the lower and middle Triassic deposits from the Svalis Dome, central Barents Sea. *Palynology*, 22, 89–141.

Vorren, T.O., Richardsen, G. & Knutsen, S.M. (1991). Cenozoic erosion and sedimentation in the western Barents Sea. *Marine and Petroleum Geology*, 8, 317–340

Worsley, D. (2008). The post-Caledonian development of Svalbard and the western Barents Sea. *Polar Research*, 27, 298–317.

Wygrala, B. P. (1989). Integrated Study of an Oil Field in the Southern Po Basin, Northern Italy [PhD]. Kernforschungszentrum Karlsruhe GmbH. 328 pp



# APPENDICES

Simulation Run Successful !  
Optimization: 0.01343 % relative difference (Largest difference: 12.67 %)

-----  
-----  
CPU Times:

Preprocessor	3	sec,	0.55	%
Pressure Analysis	3	sec,	0.55	%
Compaction	4	sec,	0.73	%
Heat Analysis	2	sec,	0.37	%
Reaction Kinetics	2	sec,	0.37	%
Mul Kinetics	0	sec,	0.00	%
Mul Kinetics	0	sec,	0.00	%
Migration	140	sec,	25.64	%
Darcy Migration	182	sec,	33.33	%
PetroCharge	36	sec,	6.59	%
Breakthrough & Fault Injection	16	sec,	2.93	%
Misc. Output	2	sec,	0.37	%
PetroCharge Final	155	sec,	28.39	%
Postprocessor	1	sec,	0.18	%
Total	9.1	min,	100.00	%
incl. Percol. (Fault)	0	sec,	0.00	%
incl. Percol. (Break Through)	1	sec,	0.18	%
incl. Overlay Output	27	sec,	4.95	%

-----  
Date/Time Tue Jul 11 11:47:41 2017  
Simulation finished at: Date/Time Tue Jul 11 11:47:41 2017

Run: 2D/3D Temperature and Pressure

Migration Method: Hybrid

Simulation started ...  
Simulation has finished!

## Appendix 1: Simulation log run for model 104

Simulation Run Successful !  
Optimization: 0.01373 % relative difference (Largest difference: 18.73 %)

-----  
-----  
CPU Times:

Preprocessor	2	sec,	0.33 %
Pressure Analysis	6	sec,	1.00 %
Compaction	4	sec,	0.66 %
Heat Analysis	2	sec,	0.33 %
Reaction Kinetics	2	sec,	0.33 %
Mul Kinetics	0	sec,	0.00 %
Migration	144	sec,	23.88 %
Darcy Migration	207	sec,	34.33 %
PetroCharge	49	sec,	8.13 %
Breakthrough & Fault Injection	0	sec,	0.00 %
Misc. Output	0	sec,	0.00 %
PetroCharge Final	183	sec,	30.35 %
Postprocessor	4	sec,	0.66 %
Total	10.1	min,	100.00 %
incl. Percol. (Fault)	0	sec,	0.00 %
incl. Percol. (Break Through)	3	sec,	0.50 %
incl. Overlay Output	20	sec,	3.32 %

-----  
Date/Time Tue Jul 11 16:36:18 2017  
Simulation finished at: Date/Time Tue Jul 11 16:36:18 2017

Run: 2D/3D Temperature and Pressure

Migration Method: Hybrid

Simulation started ...  
Simulation has finished!

## Appendix 2: Simulation log run for model 106